

# 3D Printing of Wood-Sodium Silicate Composites

A Thesis

Presented in Partial Fulfillment of the Requirements for the

Degree of Master of Science

with a

Major in Mechanical Engineering

in the

College of Graduate Studies

University of Idaho

by

Robert H. R. Carne

Approved by

Major Professor: Michael Maughan, Ph.D., PE

Committee Members: Armando McDonald, Ph.D.; Damon Woods, Ph.D.

Department Administrator: Gabriel Potirniche, Ph.D., PE

August 2022

### **Abstract**

Additive manufacturing (AM) for construction applications has grown rapidly over the past 10 years. AM, also referred to as 3D printing, in construction has primarily been done with concrete as a medium up to this point. AM has the ability to rapidly manufacture complex geometry not possible with conventional building techniques. Additionally, AM has the ability to use recycled materials and produces very little waste. Wood-based composites have yet to be used in AM for the construction industry because a method to produce high strength wood-based composites in AM has not been developed. This study details the development of an AM method for wood-sodium silicate composites (WSSC).

A 3D printer was designed and constructed utilizing a screw extruder capable of extruding wood-based composites and depositing them layer by layer onto the printer's bed. The printer is designed to use a feedstock material of wood flour and a thermoset resin binder. The samples were printed at various wood to resin ratios and were cured at various temperatures. The WSSC's adhesion to the print bed was assessed in addition to the interlayer adhesion of the printed WSSC during extrusion and after curing. A panel was successfully constructed with wood element size less than 40 mesh, at a 45:55 wood to sodium silicate weight ratio and cured for two days at 60°C. When stressed in bending, the bond between panel layers did not fail, rather failure occurred in the base material. The failures happening away from the boundary layers are consistent with other manufactured wood composites. Thus, AM can be a suitable manufacturing technique for wood-based composites based on the interlayer adhesion.

### **Acknowledgements**

Thank you to my major professor, Dr. Michael Maughan, for his support and guidance throughout my graduate education. I would like to thank Dr. Armando McDonald for his advice and aid while working with natural resources. I wish to express my gratitude to Ken Baker and Dr. Armando McDonald for their support and leadership on this project. I also wish to express gratitude to Dr. Damon Woods for his support on this project. Thank you to all my fellow graduate students who I had the pleasure of working with over the last two years. Finally, I would like to acknowledge the state of Idaho's Higher Education Research Council for funding this project through the Idaho Global Entrepreneurial Mission (IGEM) grant number IGEM 20-002.

### **Dedications**

I would like to dedicate this thesis to my father Randy and my sister Elle. I cannot thank you enough for all the support you have given me over the years. This thesis is also in loving memory of my mother Marcie. You've never stopped encouraging me to pursue my dreams

## Table of Contents

<b>Abstract</b> .....	ii
<b>Acknowledgements</b> .....	iii
<b>Dedications</b> .....	iv
<b>List of Tables</b> .....	vii
<b>List of Figures</b> .....	viii
<b>Chapter 1: Introduction</b> .....	1
<b>Chapter 2: Background and Literature Review</b> .....	3
<b>2.1 Additive Manufacturing</b> .....	3
<b>2.2 Wood-Based Composites</b> .....	6
<b>2.3 3D Printing in Construction</b> .....	9
<b>2.4 Considerations for 3D Printing Wood Feedstock</b> .....	13
<b>2.4.1 Screw Extrusion</b> .....	13
<b>2.4.2 Computer Control</b> .....	17
<b>2.4.3 Wood Waste as Feedstock</b> .....	18
<b>Chapter 3: Methods</b> .....	19
<b>3.1 Design and Fabrication of 3D Printer Frame</b> .....	19
<b>3.2 Coupling of Printer and Screw Extruder</b> .....	23
<b>3.3 Nozzle Design</b> .....	30
<b>3.4 Cooling System</b> .....	37
<b>3.5 Nozzle Rotation</b> .....	39
<b>Chapter 4: Programming and Controls</b> .....	42
<b>4.1 SmoothieBoard Configuration</b> .....	42
<b>4.2 Smoothieware Configuration</b> .....	44
<b>4.3 PronterFace G-code</b> .....	45
<b>Chapter 5: Printing Parameters</b> .....	48
<b>5.1 Wood and Resin Mixture</b> .....	48
<b>5.2 Extruder Settings</b> .....	52
<b>5.3 Curing Characteristics</b> .....	53
<b>5.4 Bed Adhesion and Removal</b> .....	54
<b>5.5 Interlayer Adhesion</b> .....	57
<b>Chapter 6: Results</b> .....	60
<b>6.1 3D Printer</b> .....	60

6.2 Extrudate Characteristics.....	61
6.3 Interlayer Adhesion .....	67
6.4 Water Soak Test.....	72
<b>Chapter 7: Summary and Conclusions .....</b>	<b>73</b>
7.1 Summary .....	73
7.2 Conclusions .....	74
<b>Chapter 8: Future Work.....</b>	<b>75</b>
<b>References.....</b>	<b>76</b>
<b>Appendix A – G-code Commands.....</b>	<b>78</b>
<b>Appendix C – Braided Hose Specifications.....</b>	<b>81</b>
<b>Appendix D – JIC Fitting Specifications .....</b>	<b>82</b>
<b>Appendix E – Threaded Die .....</b>	<b>83</b>
<b>Appendix F – V5 Nozzle .....</b>	<b>84</b>
<b>Appendix G – Rotating Head Bracket.....</b>	<b>87</b>
<b>Appendix H – Config. File for SmoothieBoard .....</b>	<b>88</b>
<b>Appendix I – G -code for Panel.....</b>	<b>91</b>
<b>Appendix J – G-code for Studded Wall.....</b>	<b>94</b>
<b>Appendix K – G-code for 2X4.....</b>	<b>95</b>

**List of Tables**

Table 2-1: Polymers and some of their properties .....	8
Table 3-1: Bill of Materials of 3D printer for WSSC.....	22
Table 5-1: Interlayer adhesion properties.....	58
Table 6-1: Density of extruded WSSC.....	61

## List of Figures

Figure 2-1: FDM 3D Printing Process.....	3
Figure 2-2: Additive manufacturing techniques and their input material state .	4
Figure 2-3: (A) Binder-jet printing process. (B) DIW of mashrabiya. (C) Two wood types printed into chessboard. (D) DCW of nut and screw. (E) Cross section of DCW printed sample .....	4
Figure 2-4: Schematic of the basic ILF process. (A) Particles deposited in thin layer. (B) Liquid adhesive is applied locally to particle bed. (C) Material is then pressed under heat to create a panel with bound and unbound bulk material. (D) Unbound bulk material is removed, and the completed panel is transferred and laminated onto stack of previously fabricated panels [4]. .....	5
Figure 2-5: Marra' s (1979) Nonperiodic Table of Wood Elements .	6
Figure 2-6: Contour crafting process .....	9
Figure 2-7: (Left) Printed pieces of castle. (Right) Fully assembled castle .	10
Figure 2-8: D-Shape printer .....	11
Figure 2-9: D-shape printed house .....	11
Figure 2-10: (1) Matrix Freeform Polymer (2) Filled and Milled Composite Core (3) Finished Façade Panel (4) Connections and Hardware.....	12
Figure 2-11: Screw extruder classifications with layouts. ....	13
Figure 2-12: Standard single-screw extruder. ....	14
Figure 2-13: Common screw configurations . ....	15
Figure 2-14: Simplified die cross-section compared to steady state pressure profile .....	16
Figure 2-15: Data collected from ten lumber companies .....	18
Figure 3-1: Initial 3D printer design.....	19
Figure 3-2: (Left) Two linear screws for Z-axis. (Right) Welded 3D printer frame with enclosed linear screws.....	20
Figure 3-3: SmoothieBoard and 24V power supply .....	21
Figure 3-4: Screw extruder .....	23
Figure 3-5: (Left) Extrudate coming out of hose attachment bolted to die. (Middle) 300psi clear reinforced hose. (Right) extruded material leaving exit of reinforced hose.....	24
Figure 3-6: 7/8" ID high-pressure braided chemical hose .....	24
Figure 3-7: (Left) Hose clamp with high-pressure hose. (Right) Failed connection. ....	25
Figure 3-8: Assembly of hose and fitting .....	25
Figure 3-9: Connection to screw extruder.....	26
Figure 3-10: Failed Connection.....	26
Figure 3-11: Fully assembled hose fitting with stiffener. Gasket not shown.....	26
Figure 3-12: First iteration of printer connection. ....	27
Figure 3-13: (A) Extruder die must be mounted at least 685.8 mm (27 in) above nozzle. (B) Extruder nozzle must be mounted in the center of the Y-axis and 228.6 mm ( 9 in) from edge.....	28
Figure 3-14: 3D printer and extruder height problem. ....	29
Figure 3-15: Transition zone between the sodium silicate and scratch grains. ....	29
Figure 3-16 Example of layered extrudate. ....	30
Figure 3-17: (Left) Nozzle V1 with two hose connection types. (Right) Exit of nozzle.....	30
Figure 3-18: Nozzle, hose, and die attached together with hose clamps. ....	31



Figure 3-19: (Left) Nozzle filled with material at failure. (Right) Deformed material at exit of nozzle. .....	31
Figure 3-20: (Left) V2 nozzle halves. (Right) Exit of nozzle.....	32
Figure 3-21: Successful rectangular extrusion. ....	32
Figure 3-22: Failed V2 nozzle.....	33
Figure 3-23: V3 aluminum nozzle with rabbit joint. ....	33
Figure 3-24: V3 nozzle with rectangular extrudate.....	34
Figure 3-25: V4 nozzle with JIC fitting. ....	34
Figure 3-26: (Left) WSSC cured inside nozzle. (Right) Residue left behind after cleaning. ....	35
Figure 3-27: Extruded WSSC with shark skin.....	35
Figure 3-28: V5 nozzle made of 1018 steel. ....	36
Figure 3-29: (Top) Extrudate at room temp. (Bottom) Extrudate at 52.5°C. ....	37
Figure 3-30: Cooling system .....	38
Figure 3-31: (Left) No cooling. (Right) With cooling.....	38
Figure 3-32: (Left) Nozzle in home ( 0-degree) position. (Right) Nozzle in 90-degree position.....	39
Figure 3-33: (Left) 63 N holding force linear actuator. (Right) 957 N holding force linear actuator. ..	40
Figure 3-34: Added gussets to bracket to support larger actuator.....	40
Figure 3-35: 957 N linear actuator with nozzle in 90-degree position.....	41
Figure 4-1: 3D printer control system layout. ....	42
Figure 4- 2: SmoothieBoard pin configuration.....	43
Figure 4-3: PronterFace user window. ....	45
Figure 4-4: Printer Check G-code .....	46
Figure 4-5: Printer connected to Pronterface. ....	46
Figure 4-6: G-code selection window.....	47
Figure 4-7: Running print file.....	47
Figure 5-1: Less than 40 mesh wood flour being sieved. ....	48
Figure 5-2: WSSC placed in food processor.....	49
Figure 5-3: Mixture with added water on parchment paper .....	49
Figure 5-4: (Left) Pour-over mixing before curing. (Right) After curing. ....	50
Figure 5-5: (Left) Stored at room temperature. (Right) Stored in stand-up freezer. ....	50
Figure 5-6: Green food coloring placed on top of material.....	51
Figure 5-7: Zero-compression and compression screws.....	52
Figure 5-8: WSSC water soak test.....	53
Figure 5-9: Nozzle/Print-Bed relationship.....	54
Figure 5-10: (Left) Extrudate freely coming out as round extrudate. (Right) Rectangular extrudate curling up from bed. ....	55
Figure 5-11: Printed material held at beginning of print with second layer. ....	55
Figure 5-12: (Left) Printed Extrudate left on aluminum bed. (Right) Blue painters tape applied to bed surface. ....	56
Figure 5-13: (Left) Extruded Rod. (Right) Rods broken into pieces.....	57
Figure 5-14: (Left) Pressed ball extrudate. (Right) Vertically pressed extrudate.....	58
Figure 5-15: 90-degree layer orientation. ....	59

Figure 5-16: (Left) Vertical layering. (Right) Horizontal Layering .....	59
Figure 6-1: Schematic representation of 3D printer for WSSC. ....	60
Figure 6-2: Photograph of 3D printer for WSSC. ....	60
Figure 6-3: Fiber configuration of round extrudate. ....	61
Figure 6-4: Fiber configuration of rectangular extrudate. ....	62
Figure 6-5: (A) Fresh extrudate. (B) Extrudate held at room temperature. (C) Extrudate stored in freezer. ....	62
Figure 6-6: Water added to mixture unable to extrude. ....	63
Figure 6-7: Sodium silicate and water mix leaking from die. ....	63
Figure 6-8: (Left) Liquid mixture (Center) Hand Mixed (Right) Binder Jetting .....	64
Figure 6-9: (Left) Cured mixture with water added. (Right) Broken wood composite. ....	64
Figure 6-10: Ink jetting of sodium silicate onto wood flour. ....	65
Figure 6-11: Extrudate with added green food coloring. ....	65
Figure 6-12: (Left) Side view of extrudate interaction with bed. (Center) Front view. (Right) Back view. ....	66
Figure 6- 13: (Left) Segment separates at boundary layer. (Right) All four sections of extrudate separated. ....	67
Figure 6-14: Failed interlayer connections .....	67
Figure 6-15: Layers separate during curing. ....	68
Figure 6-16: Cross layering .....	69
Figure 6-17: 3D printed material in both X and Y directions. ....	69
Figure 6-18: Side-by-side layering of WSSC with interlayer adhesion. (Left) Top. (Right) Bottom. ....	70
Figure 6-19: Failure occurred in the base material not at layer boundary. ....	70
Figure 6-20: 3D printed panel .....	71
Figure 6-21: Dissolved WSSC cured at room temperature. ....	72
Figure 6-22: Average percentage change of weight and thickness of panel samples before and after soaking. ....	72

## Chapter 1: Introduction

Additive manufacturing for construction applications has grown rapidly over the past 10 years. Taking up only 3.1% of the 3D printing application market [1], the engineering and construction industry's global annual revenue is valued at \$10 trillion [2]. A cornerstone of the globe's economy, engineering and construction account for nearly 6% of GDP. Integrating additive manufacturing or 3D printing into the construction industry will help utilize waste material from natural resources and create a more sustainable and green building product.

3D printing in construction has primarily been done with concrete as a medium up to this point. Companies such as XtreeE, CyBe, Apis-Cor, and Mudbots have been using concrete blends to manufacture houses, large-scale art installments, and other infrastructures using layer-by-layer additive manufacturing [3]. Concrete has dominated the 3D printing construction market because of its flow characteristics and curing properties. The popularity of using renewable resources such as wood has gained traction in additive manufacturing as it can help make AM processes more affordable and reduce the environmental impact of today's constructions practices [4]. The construction industry accounts for 37% of energy derived CO<sub>2</sub> emissions, most of this comes from material production [5]. Modern lumber mills only convert about 56% of the wood volume into usable lumber [6].

Wood-based composites have been around for decades. Plywood, OSB, particleboard, laminated veneer lumber (LVL), and glue-laminated timber are some of the most common wood-based composites on the market today. The use of wood-based composites in additive manufacturing has the potential to revolutionize the 3D printing construction market. One of the biggest attractions of 3D printing in construction is waste reduction. Compared to traditional manufacturing methods, the waste produced in 3D printing is almost zero. The use of scrap and waste materials from other industries gives wood-based composites in 3D printing an advantage over other mediums (such as concrete). However, extruding wood-based composites for 3D printing needs further study. Unlike molten plastics or wet concrete, current wood-based composites do not flow or bind well to one another once extruded. These challenges must be solved before wood-based composites can be fully utilized in the 3D printing construction industry.

The purpose of this research was to give proof of concept of the methodology to use 3D printing in construction applications utilizing waste wood elements and sodium-silicate. The final outcome of the research is to develop a reliable process for 3D printing house walls, floors, and roofs on a horizontal printing bed. This process can then be used to manufacture modular residential homes

for low cost or provide other opportunities. This study presents the development of a method to 3D print wood-based composites for the purpose of additive manufacturing in the construction industry.

## Chapter 2: Background and Literature Review

The following chapter will provide a review of additive manufacturing and existing techniques utilizing wood filler, wood composites, and existing additive manufacturing techniques for construction applications.

### 2.1 Additive Manufacturing

Additive manufacturing (AM), commonly referred to as 3D printing, is a process that most commonly extrudes material and builds parts up layer by layer through a computer guided nozzle as shown in Figure 2-1. Originally used for prototyping, 3D printing has expanded into many industries including aerospace, automotive, healthcare and even construction [7]. There are many types of AM processes and they can be classified based on the form of the input material, as summarized in Figure 2-2 [8]. Fused Deposition Modeling (FDM) is one of the most frequently used AM process for both prototypes and final parts [9]. This AM process relies on thermal fusion to bond each layer to the one beneath it. There are some polymer-based composites with less than 50% wood content that use this process. In most cases wood flour is combined with PLA at a 70:30, wood to PLA ratio, resulting in a weak, high-cost material as PLA is ten times more expensive than wood flour. Unfortunately, the low ratio of wood and use of low-strength materials, means these composites are not appropriate for construction applications.

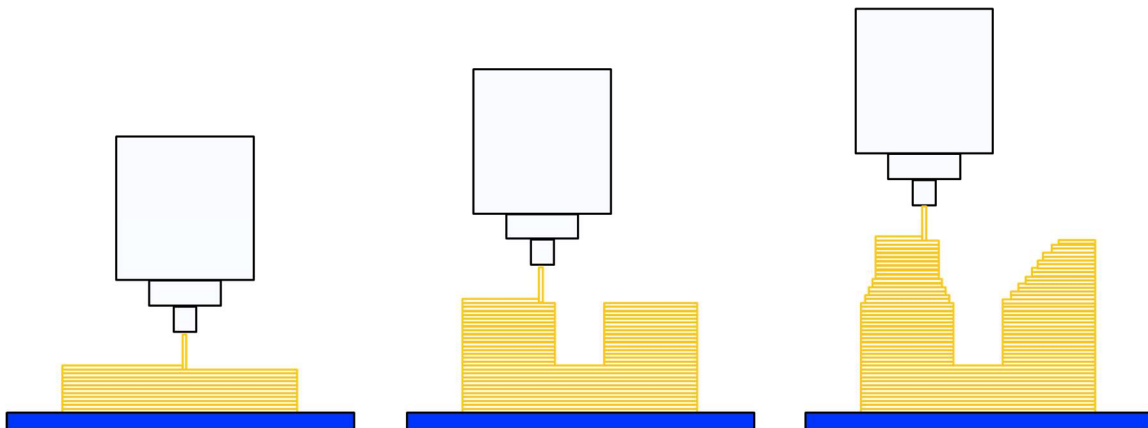


Figure 2-1: FDM 3D Printing Process.

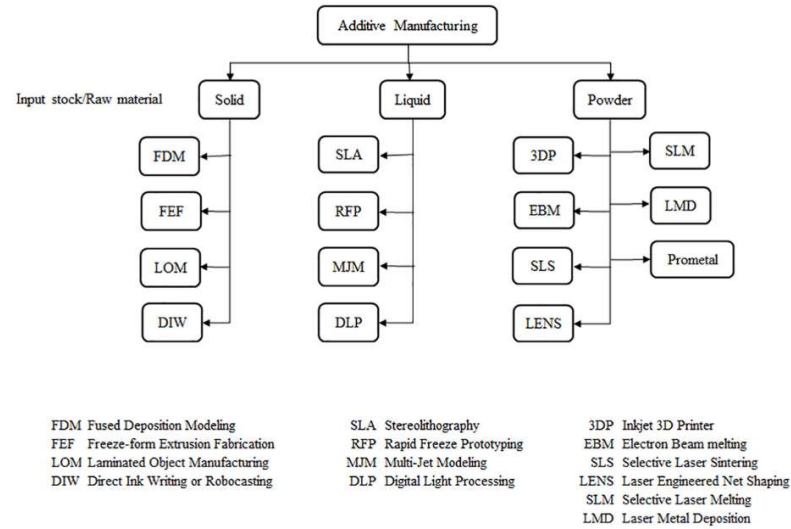


Figure 2-2: Additive manufacturing techniques and their input material state [8].

Only solid and powder input material will be discussed as the wood filler cannot be in a liquid state. A novel AM approach for wood presented in *Additive Manufacturing of 3D Structures Composed of Wood Materials* [10] utilizes two binder jetting techniques: direct ink writing (DIW) and direct cyro writing (DCW). DIW is done under ambient conditions while DCW uses a cold plate and is frozen in a controlled fashion. In extrusion-based technologies, material is extruded through a nozzle to build up a 3D object. In binder jet technology, ink droplets are jetted out and can serve as a binder at desired locations (binder-jet printers) [10]. A schematic illustrating the DIW and DCW technique is shown in Figure 2-3.

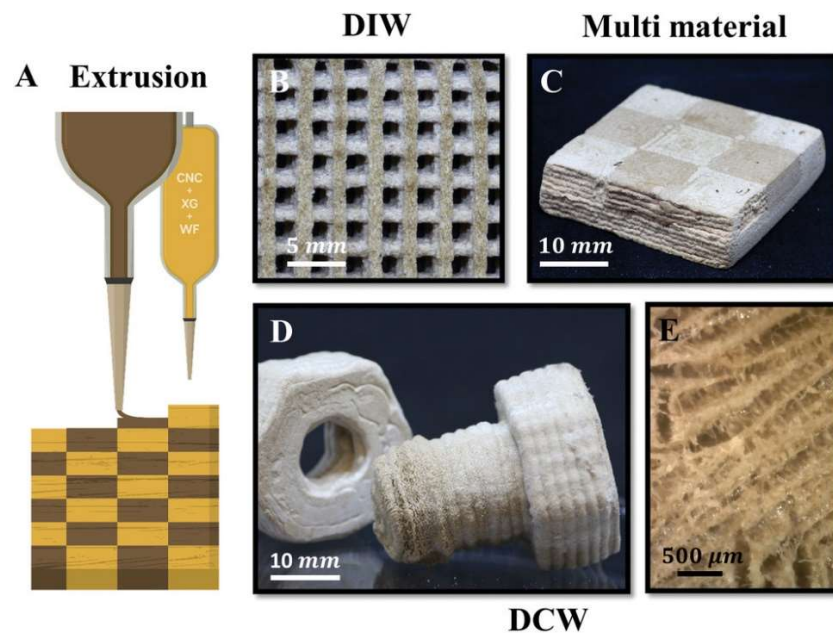
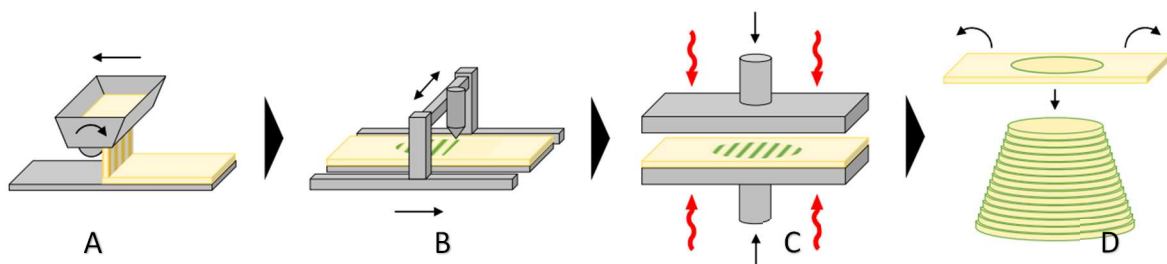


Figure 2-3: (A) Binder-jet printing process. (B) DIW of mashrabiya. (C) Two wood types printed into chessboard. (D) DCW of nut and screw. (E) Cross section of DCW printed sample [10].

Individual layer fabrication (ILF) was designed with the use of wood in mind. The aim of ILF is to obtain additively manufactured wood composite parts with material properties comparable to those of conventionally fabricated wood particle composite boards [4]. ILF is a combination of two processes, binder jetting, as mentioned above, and sheet-lamination. Sheet-lamination is an AM process that stacks and laminates thin sheets of material up into a desired shape. Lamination occurs through chemical bonding or ultrasonic welding. The final shape is achieved by either laser cutting or a computer numerical control (CNC) machine [11]. ILF also introduces mechanical pressure to the different sheets after the binder's application and before layering the sheets for lamination. The process of ILF is demonstrated in Figure 2-4.



*Figure 2-4: Schematic of the basic ILF process. (A) Particles deposited in thin layer. (B) Liquid adhesive is applied locally to particle bed. (C) Material is then pressed under heat to create a panel with bound and unbound bulk material. (D) Unbound bulk material is removed, and the completed panel is transferred and laminated onto stack of previously fabricated panels [11].*

## 2.2 Wood-Based Composites

During the last 70 years, use of composite lumber and panels has grown from limited applications in specialty markets to full integration into commodity and specialty markets such as framing, subflooring, roof and wall sheathing, corner bracing, concrete forming, paneling, cabinetry, countertop stock, underlayment, and siding [12]. Figure 2-5 shows the different elements a tree can be broken down into after harvest. Composite wood products combine a level of refined wood element and a polymer to create resource-efficient structural and nonstructural materials.

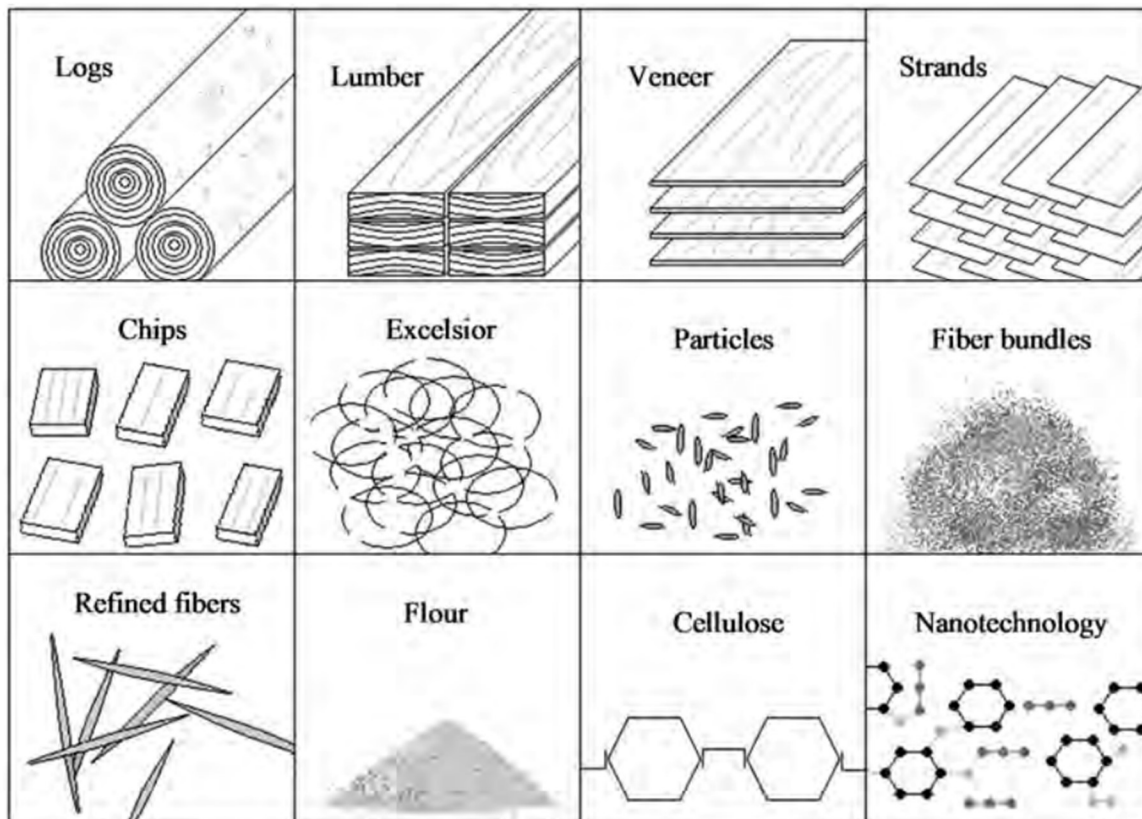


Figure 2-5: Marra's (1979) Nonperiodic Table of Wood Elements [12].

Looking at some of the structural products of natural fiber composites, they consist of both small fiber composites and veneers. Veneers are created by heating the log and placing it on a veneer peeler to create a thin sheet of wood. Laminated veneer lumber (LVL) and plywood both utilize this natural fiber. For LVL, the grain of veneers is placed parallel to the grain in the long direction, while plywood is made of veneer sheets that are placed at 90-degree orientations to one another. LVL billets are then milled to the desired dimensions depending on the end-use application such as headers and beams, hip and valley rafters, scaffolding planking, and flange material for



prefabricated wood I-joists. Most LVLs and plywoods use Douglas fir, southern pine, or yellow poplar woods as filler and phenol-formaldehyde (PF) or resorcinol formaldehyde (RF) as the adhesive.

Natural fiber composites using particles, fiber bundles, refined fibers, and flour are more prevalent in non-structural applications. Particleboard is one such composite that was first introduced around 1900 and originally made from sawmill residues (sawdust, shavings) and animal-based adhesives. Commercial production and use of modern wood particle board did not start until the 1940s. Urea formaldehyde (UF) has been used as the binder of wood-based particleboard since the beginning. Hardboard is a generic term for a panel manufactured primarily from inter-felted lignocellulose fibers consolidated under heat and pressure in a hot press to a density of greater than  $0.5 \text{ g/cm}^3$ . The inter-fiber bond is primarily achieved through the action of lignin. Other materials may be added during manufacturing to improve properties, such as stiffness, hardness, finishing properties, resistance to abrasion and moisture, as well as to increase strength, durability, and utility. Hardboard is used in wall and ceiling paneling, furniture, automotive panels, embossed panels, and has the ability to be post formed. Up until medium-density-fiberboard (MDF) was first produced in 1965 using a dry forming process, fiberboard had been made using a wet forming processes since 1898 to produce things like soft and hardboard. The density of MDF ranges from  $350\text{-}800 \text{ kg/m}^3$  and has a smooth finish and is highly machinable.

Polymers can be categorized into thermosets and thermoplastics. Thermosets are polymers that undergo a chemical reaction during the curing process and normally transform from a liquid to a solid when the addition of a second material such as a catalyst or curing agent initiates the chemical reaction and cures. Exposing thermosets to high heat will cause the material to degrade, not melt. Thermoplastics on the other hand are melt-processable plastics. Heat is added to bring the temperature of the thermoplastic above its melting point to soften it enough, so the thermoplastic liquefies. When the heat source is removed and the temperature drops below its melting point, the thermoplastic solidifies. Thermoset and thermoplastic materials each have their unique set of properties and position in the market. Thermoplastics tend to be tougher than thermoset and can have better chemical resistance [13].

Biopolymers are polymers obtained from natural resources [13]. Biopolymers vary among their hardness, melt flow indices, impact properties, and decomposition. Biopolymers can be thermoset or thermoplastic. Some of the bio-degradable polymers are cellulosic plastics, polylactides, starch plastics, polyhydroxyalkanoates (bacterial polyesters), and soy-based plastics,

these types of polymers are continuously being developed. Additional thermoplastic, thermoset, and biopolymers can be seen in Table 2-1 [13].

Table 2-1: Polymers and some of their properties [13]

	Polymers	Density (g/cm <sup>3</sup> )	Elongation (%)	Tensile strength (MPa)	Young's modulus (GPa)
Thermoplastic	Acrylonitrile butadiene styrene (ABS)	1.0–1.1	270	47	2.1
	Cross-linked polyethylene (PE)	0.9	350	18	0.5
	Ethylene vinyl acetate (EVA)	0.9–1.0	750	17	0.02
	High-density polyethylene (HDPE)	0.9–1.0	150	32.0–38.2	1.3
	High-impact polystyrene (HIPS)	1	2.5	42	2.1
	Low-density polyethylene (LDPE)	0.9	400	10.0–11.6	0.2–0.3
	Nylon 6 (PA 6)	1.1	60	81.4	2.8
	Nylon 6,6 (PA 6,6)	1.1	60	82.7	2.8
	Polycarbonate (PC)	1.2	200	69	2.3
	Polyethylene terephthalate (PET)	1.5–1.6	300	55.0–159.0	2.3–9.0
	Polyether ether ketone (PEEK)	1.3–1.5	1.6–50.0	92.0–95.0	3.7–24.0
	Poly ether ketone (PEK)	1.2–1.4	20	100.0–110.0	3.5
	Poly methyl methacrylate (PMMA)	1.1–1.2	2.5	72.4	3
	Polypropylene (PP)	0.9–1.3	80	35.8	1.6
	Thermoset	Polystyrene (PS)	1.04	1.6	34
Polyvinyl chloride (PVC)		1.3–1.5	50.0–80.0	52.0–90.0	3.0–4.0
Rigid thermoplastic polyurethane (RTPU, PUR-RT)		1.1	5	75	4
Epoxy (EP)		1.2–1.3	1.3	600	80
Melamine formaldehyde (MF)		1.5–1.6	0.6	65	12
Phenol formaldehyde (PF)		1.2	1.2	45	6.5
Rigid thermoset polyurethane (RPU)		1.2	90	60	2.2
Biopolymers	Unsaturated polyester (UPE)	1.1	2	60	3.4
	Urea formaldehyde (UF)	1.5–1.6	0.8	65	9
	Polyurethane rubber	1.2–1.3	300.0–580.0	39	2.0–10.0
	Poly-lactic acid (PLA)	1.2–1.3	2.1–30.7	5.9–72.0	1.1–3.6
	Polyhydroxyalkanoates (PHA)	1.2–1.3	2.0–1200.0	10.0–39.0	0.3–3.8
	Polyhydroxybutyrate (PHB)	1.2	1.56–6.0	24.0–40.0	3.5–7.7
	Poly-3-hydroxybutyrate (P-3-HB)	1.3	0.4–6.0	40	3.5
Biopolymers	Poly-3-hydroxybutyrate-co-3-hydroxyvalerate (P-3-HB-3 HV)	0.2–0.3	1.6–20.0	23.0–40.0	3.5
	Poly-3-hydroxybutyrate (P-3-HB)	1.2	1000	104	—
	Polycaprolactone (PCL)	1.1	700	16.0–23.0	0.4

Standard manufacturing for panels such as the ones mentioned above all use similar methods to produce each panel. Each panel's refined wood elements are dried to control moisture content before blending with a desired resin adhesive. After blending the panels are formed into mats and then pressed in large hot or cold presses ranging in size from single opening to 16-opening and larger presses. The pressing time each panel varies depending on the panel's thickness [12]. Although other materials such as concrete have been utilized in AM for construction, the manufacturing of wood composites for construction applications using AM has yet to be developed.

### 2.3 3D Printing in Construction

The research and practice of AM in construction is currently limited to four processes worldwide: contour crafting, concrete printing, binder jetting, and C-Fab or cellular fabrication [14].

Contour Crafting (CC) is a new AM process using concrete for construction using layered fabrication technology [15]. Unlike FDM, CC relies on the chemical and mechanical bonds between layers. The key feature of CC is the use of two trowels, which function as two solid planar surfaces to create surfaces on the object being fabricated that are exceptionally smooth and accurate (Figure 2-6).

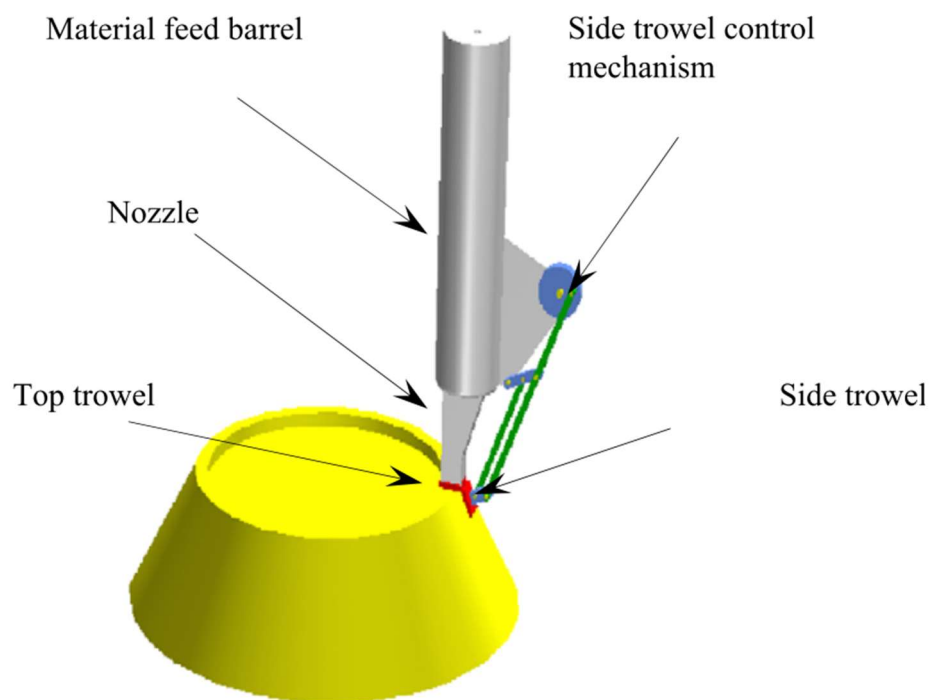


Figure 2-6: Contour crafting process [15].

Artists and craftsmen have effectively used simple tools such as trowels, blades, sculpturing knives, and putty knives with one or two planar surfaces for forming materials in paste form since ancient times [15]. There have been numerous cases of buildings being printed using contour crafting. Figure 2-7 shows one of the most notable cases where a castle was poured using a mixture of cement and sand. The material used in his printer was a mix of cement and sand. The whole building was printed on a single run, except for the towers, which were printed separately and affixed to the building [16].



*Figure 2-7: (Left) Printed pieces of castle [17]. (Right) Fully assembled castle [16].*

Contour crafting techniques demonstrate post-extrusion deformation allowing the material to be molded into the desired final shape or surface finish. Concrete printing, similar to contour crafting, does not have the two trowels attached to the nozzle. The finishing of the surface is done manually by workers as other parts of the structure are being printed. The viscosity of concrete for printing is significantly higher than the viscosity of the wood-composite extrudates allowing for easy transport and deposition for the material.

D-Shape Enterprises uses binder jetting AM for architecture. The D-shape printer uses a process of alternating layers of granular material and writing on them with an appropriate “ink binder” that turns the granular material into a shape. Binder jetting and DIW are both mentioned in chapter 2.1. D-Shape printers deposit granular material and fibers in a range of diameters and any binder having a viscosity between water and a slurry. The nozzles of the D-Shape’s printer head deposits drops of the binder’ whose volume are about 100 times bigger than existing inkjet printer heads. Figure 2-8 shows the D-Shape’s structure which supports a peripheral frame raised along four columns. On the frame there are two gantries, one of which distribute and spreads a granular material, while the second holds a multi-binder-jetting print head [18].



*Figure 2-8: D-Shape printer [18].*

D-shape successfully 3D printed the first one-shot-printed house. It contains the bathroom and a kitchen space and bedroom. Printing the house took three weeks. The printed house can be seen in Figure 2-9.



*Figure 2-9:D-shape printed house [18].*

Cellular Fabrication or C-Fab is a patented process by Branch Technologies. C-Fab uses a freeform polymer matrix that is 3D printed to employ geometric optimization principles to generate architectural components with maximum strength and minimal material use [19]. Branch Technologies offers two primary ventilated rainscreen systems, the BranchClad and StoPanel 3DP system. These panel's matrix materials, density, color, and embedded technology can all be customized. The matrixes are entirely 3D printed using 6-axis robotic arms. The openings in the

matrix are then filled with a composite core and milled down to the desired shape. The panels are then finished in Glass Fiber Reinforced Concrete (GFRC) or synthetic stucco before being shipped to site. Once on site the products' adaptability allows for connections to industry-standard rainscreen hardware as well as to fully bespoke engineered structural attachments. Branch Technologies' solution to connecting each panel include embedded frames that span from floor to floor for the larger panels or 3D printed mounts that attach directly to standard wall systems [19]. The structure of the panels is shown in Figure 2-10.



*Figure 2-10: (1) Matrix Freeform Polymer (2) Filled and Milled Composite Core (3) Finished Façade Panel (4) Connections and Hardware [19].*

The use of screw extrusion and computer-controlled printers are seen across all of the additive manufacturing processes mentioned above. Screw extruders are ideal for continuous processes making for efficient manufacturing. The design of each screw extruder is unique to its own application. The use of computer-controlled devices minimizes labor cost and allows for unique and accurate designs.

## 2.4 Considerations for 3D Printing Wood Feedstock

### 2.4.1 Screw Extrusion

Extrusion is the process of forcing a material through a die or opening to create a desired profile. Extrusion can be accomplished with a ram, rotation screw, or other feed mechanism. Screw extruders are classified into single, twin, or multi-screw designs. The first single-screw extruder for polymers was produced in 1951 in Japan for extrusion of wire/cable coating with low density polyethylene [20]. Figure 2-11 shows common single screw extruder layouts used in the polymer industry.

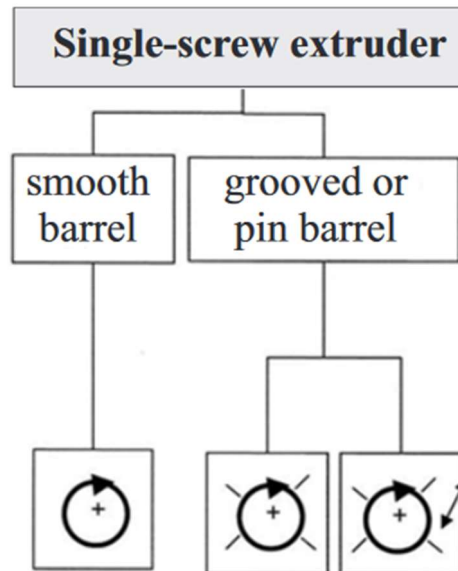


Figure 2-11: Screw extruder classifications with layouts [21].

For single-screw extrusion of polymers, raw materials such as powder or pellets are placed into a hopper that feeds a single screw rotating at a predetermined speed within a cylindrical barrel. The rotation of the screw continuously pushes the material through the three main sections of the extruder before exiting from the die. The screw begins to taper in the melt section, which causes the melting polymer to shear. Screw and die design play a key role in how the extruder functions. Figure 2-12 illustrates the standard design for a single-screw extruder.

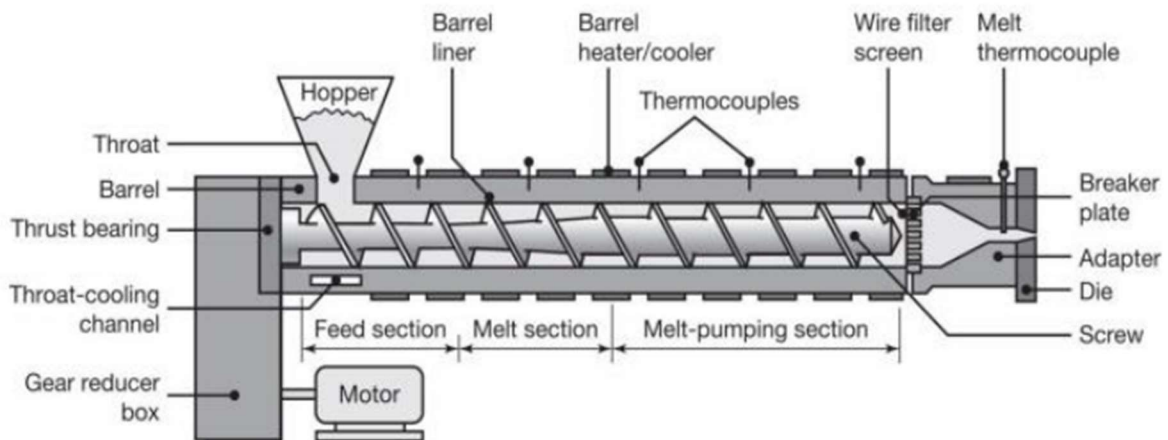


Figure 2-12: Standard single-screw extruder [21].

Screw design is dependent on the processing requirements. The design of the taper and pitch of the screw determines the compression ratio or ratio between the initial and final channel depths. Different screw configurations will provide different shearing conditions and pressure profiles that are uniquely suited for the production of various products. The typical compression ratio of a screw is between 1:2 and 1:4 while the typical length-to-diameter ratio of the screw is between 20:1 to 30:1 [22]. Figure 2-13 shows common screw configurations available, but it should be noted an unlimited number of screw configurations can be achieved.



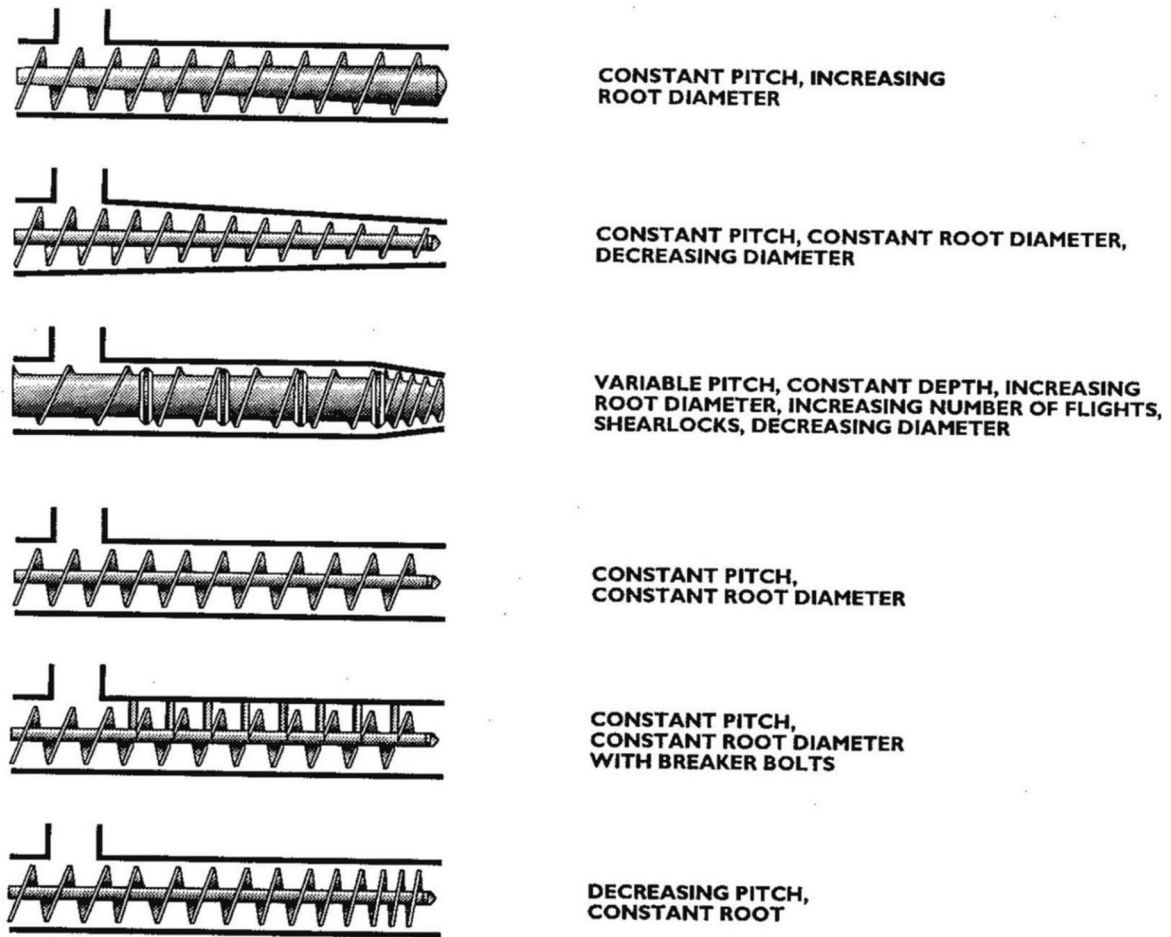


Figure 2-13: Common screw configurations [23].

Dies for extrusion provide compression of the material and determine the final profile of the extrudate. Die designs are regularly developed through capillary rheology and experimental testing. Die design affects the extrusion by inducing pressure to create flow. Die design optimizes flow rate, material density and required motor torque. The general expression relating the flow and pressure inside the die is known as the die characteristic and is written as:

$$Q_{die} = Kp \quad (1)$$

Where  $Q_{die}$  is the flow through the die,  $p$  is the pressure at the die inlet, and  $K$  is a function of die geometry. Typically,  $K$  is determined experimentally, however, for circular die cross-sections there is a closed-form solution [21]. This equation is written as:

$$K = \frac{\pi D_d^4}{128\eta L_d} \quad (2)$$

Where  $D_d$  is the diameter of the die-opening, and  $L_d$  is the length of the die land. If die and extruder characteristic equations are known, then the pressure and flow rate of the system can be solved algebraically [3].

Once the material leaves the die, it does not typically retain the exact shape of the die's opening. This is because the material leaving the die is usually soft and the pressure, in the die is relieved. Because of this relieved pressure the material often swells. The swelling of the extrudate is called die swell. Die swell characteristically increases if any of the following happen: extrusion speed increases, die dimensions decrease, melt temperature decreases, or die land length to diameter ratio decreases [25]. Figure 2-14 illustrates a simple die cross-section and the typical pressure profile through the die. As shown, the pressure on the material begins to decrease once it enters the head of the die and eventually drops to zero at the die exit [3].

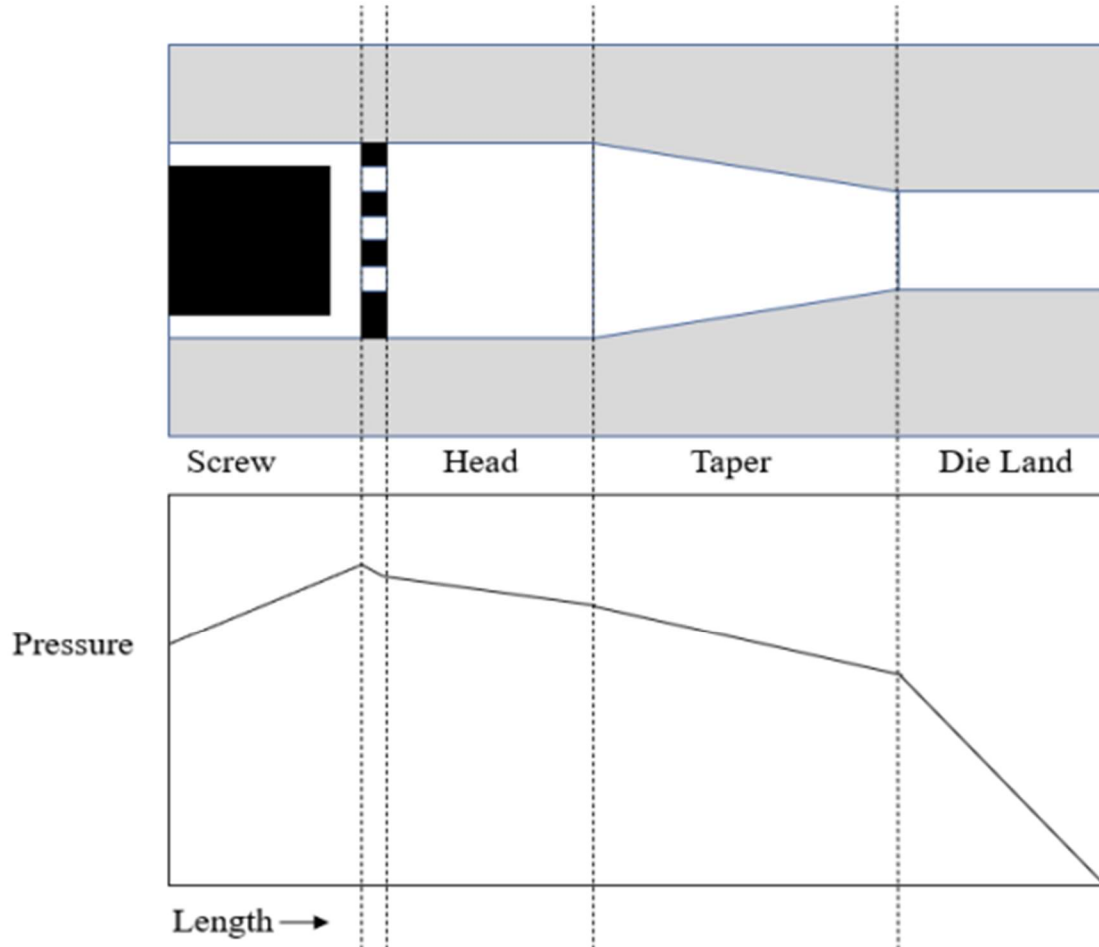


Figure 2-14: Simplified die cross-section compared to steady state pressure profile [3].

### 2.4.2 Computer Control

G-code is the simple programming language for CNC machines and 3D printers. It consists of lines of code that are organized in blocks. Each block controls one operation, such as a depositing material in a specific path [24]. Every G-code command is a letter/number combination. Each corresponds to a different type of action for the machine to execute. Basic G-code commands can be found in Appendix A.

To execute G-code commands a software host is needed. PronterFace is a fully featured graphical user interface (GUI) host for building, reading, and sending G-Code to the 3D printers stepper motors controlling the X, Y, and Z-axes as well as other features. The standard features ran by g-code on a 3D printer are stepper motor direction and speed, fan on/off, bed temperature, and extruder speed. Note that just specifying a command such as G00 does not cause any motion to happen. The “G” command tells the controller what type of motion is expected when a move command is initiated. In order for the motion to happen, a destination needs to be specified using “X”, “Y”, and “Z” commands to express the coordinate system axis. The direction of movement is typed first followed by the position from home. For example, in SI units a position that is 100 mm in the X-direction, 200mm in the Y-direction, and 10mm in the Z-direction is written as: X100 Y200 Z10. The speed that the tool head travels is dictated by the “F” command followed by the speed in mm/min. The G-code line: G01 X100 Y200 Z10 F28, would move the tool head in a straight line to the position of 100 mm, 200 mm, 10 mm (X, Y, Z) at a rate of 28 mm/min.

### 2.4.3 Wood Waste as Feedstock

Lumber mills only convert 56% of timber harvested into good products or lumber, meaning that 44% of logs processed are turned into waste [6]. There are two types of waste associated with lumber production, avoidable and unavoidable wastes. Unavoidable wastes are those wood wastes that cannot be avoided or prevented even were the saw kerf is minimal, and the mill workers are efficient. These include sawdust, inconvertible slabs, and strips. Avoidable wastes are caused by a lack of pre-inspection of trees and logs, inadequate saw maintenance, and poor harvesting techniques, which result in residues in the forest in the form of branches, tree crowns, off cuts, twigs, stumps, small diameter sized timbers etc. Others include substandard lumbers which are inaccurately processed or converted as a result of faults on both the bandmills and circular resaw machines. Both avoidable and unavoidable wood wastes generated during harvesting and conversion are enormous and, when pooled together, can be used in the production of new building materials [6].

Data collected from ten lumber companies shows, one metric ton of lumber emits between 41 and 726 kgCO<sub>2</sub>. Approximately 63% of the carbon emissions are produced at the sawmill and 34% during transportation to the consumer [25]. Figure 2-15 breaks down the carbon emissions, embodied energy, and residues over the life cycle of lumber.

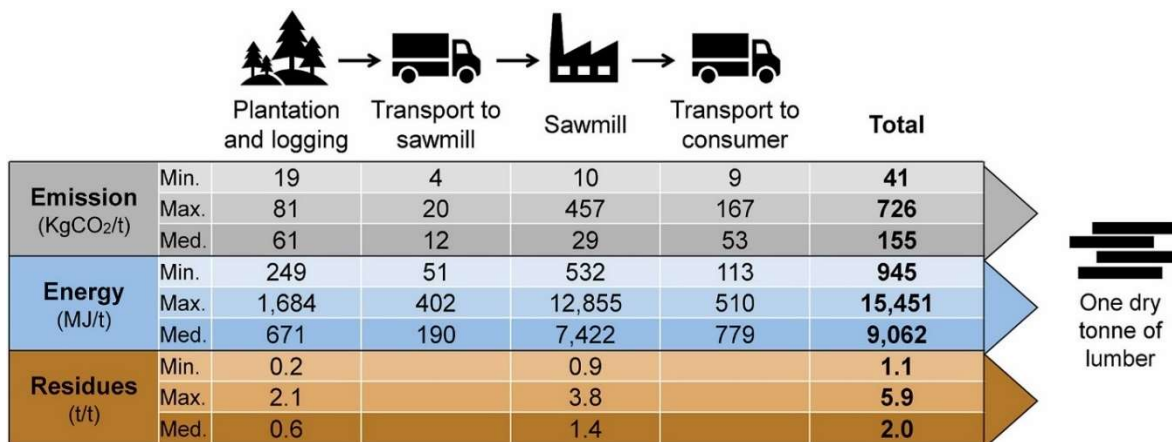


Figure 2-15: Data collected from ten lumber companies [25].

As mentioned previously in section 2.1, PLA is a material derived from biomass that has been utilized with wood flour. Several studies have incorporated low levels of wood filler with PLA in a range of 5% to 10% ratio [26]–[28]. The low wood content, high cost of PLA and the tendency for thermoplastics to creep make these composites unsuitable for construction applications.

## Chapter 3: Methods

The methodology to use wood-based composites in AM for construction applications was explored in this study. Since there is no established field for using wood in AM construction applications, a 3D printing technique had to be created. After a 3D printer was developed, it was used to produce samples of wood-based composites through different additive manufacturing techniques and examined using multiple methods. The wood-based composite was a mixture of fine wood flour and a thermoset resin of sodium silicate to be referred to as wood-sodium silicate composite (WSSC). The deposition of extrudate, layer-to-layer connections, and ratio of wood flour to resin were factors examined. Once printed, the samples must dry for the resin to fully cure. Various curing and drying methods were performed on the extruded composite samples. Various curing and drying methods were performed on the printed composite samples.

### 3.1 Design and Fabrication of 3D Printer Frame

The purpose of developing a 3D printer for wood-based composites is to demonstrate wood-based AM construction. An initial 3D printer frame was designed in Solidworks by University of Idaho undergraduate Evan Allen (Figure 3-1) with the goal of printing approximately 650 mm by 950 mm demonstration panels. A frame large and strong enough was needed to accommodate a panel of this size. Detailed files of the 3D printer frame are shown in Appendix B.

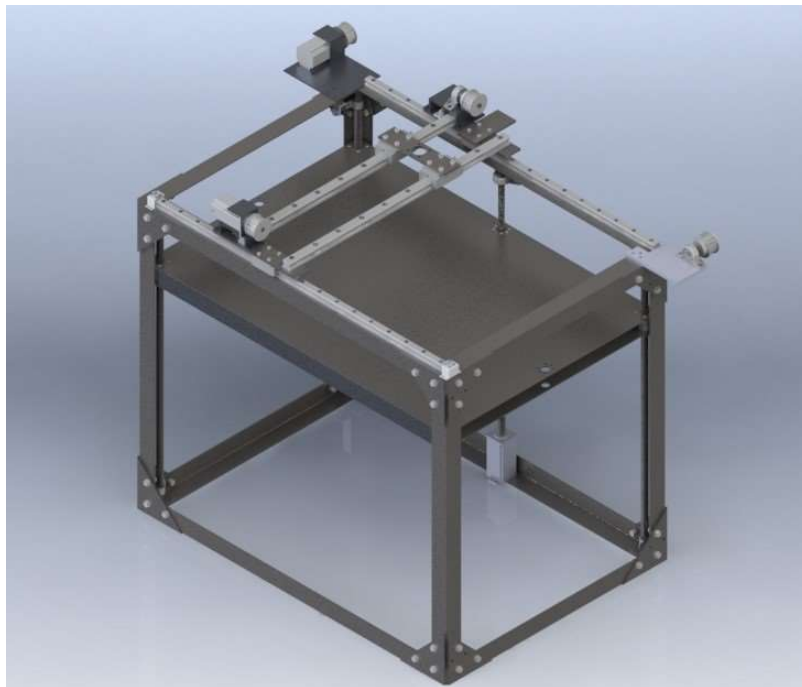


Figure 3-1: Initial 3D printer design.

The initial design consisted of a bolted together steel frame with a belt and pulley system for the X- and Y-axes and a single liner screw for the Z-axis. This design was modified to meet various constraints. The final design for the frame/gantry system consisted of one 750 mm enclosed liner screw for the X-axis, two 1000 mm enclosed linear screws for the Y-axis, and two 825 mm non-enclosed liner screw for the Z-axis. Enclosed linear screws were used to limit the amount of dust and debris that can obstruct the path of the X- and Y-axis. Two linear screws for the Z-axis were necessary to maintain bed alignment and provide enough torque to support the weight of the panels. The X- and Y-axis linear screws are powered by NEMA 23 stepper motors, and the Z-axis is powered by a NEMA 34. The bolted together frame was also changed to a welded steel frame with dimensions 1067 mm x 762 mm x 915 mm (L x W x H). The print bed is made from a 3 mm thick aluminum sheet with aluminum c-channel bolted to it underside of the bed. Four polished steel rods attached at the corners of the printer frame with vibration dampeners were used to guide four 121 mm flange-mounted linear ball bearings mounted to the print bed. These guides leveled and aligned the print bed with the frame and Z-axis linear screws. A schematic and photo of the final 3D printer frame is shown in Figure 3-2.



Figure 3-2: (Left) Two linear screws for Z-axis. (Right) Welded 3D printer frame with enclosed linear screws.

The 3D printer's stepper motors were controlled using a SmoothieBoard V5 wired to a 24v power supply shown in Figure 3-3. Table 3-1 below contains the full bill of materials for the 3D printer frame.

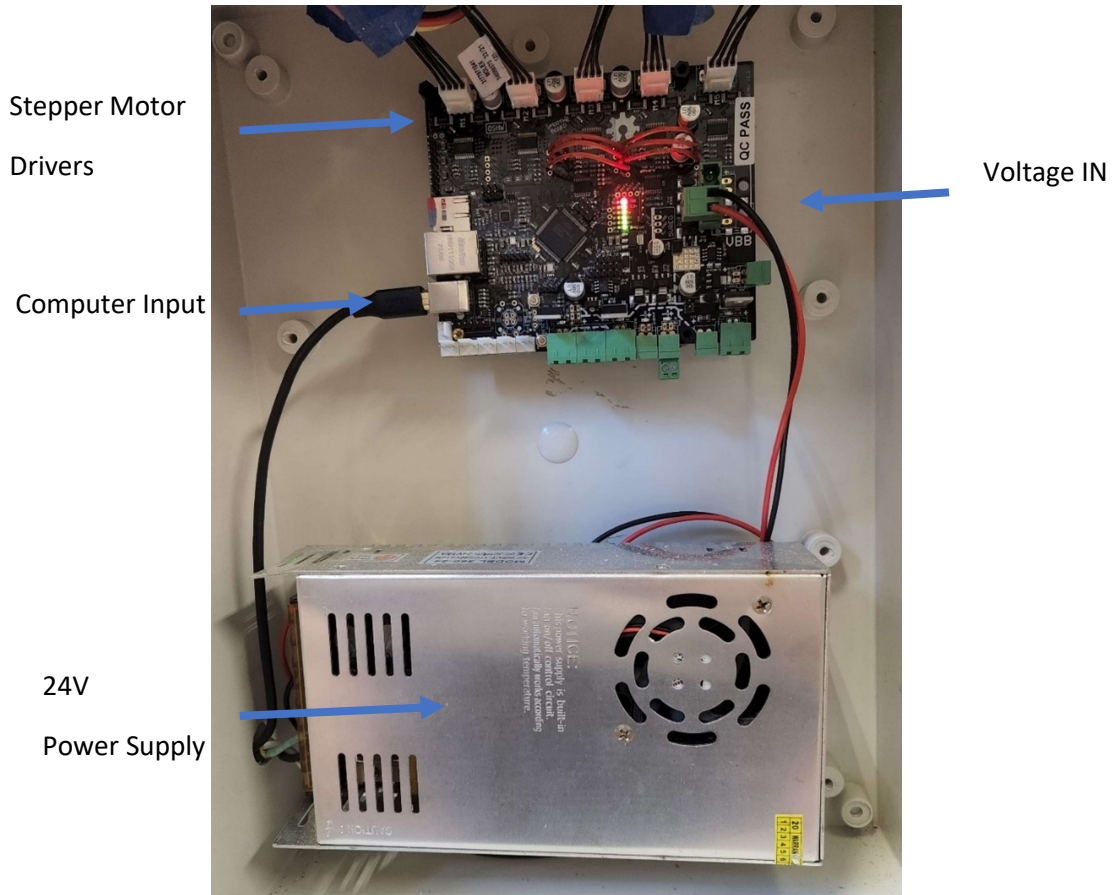


Figure 3-3: SmoothieBoard and 24V power supply

Table 3-1: Bill of Materials of 3D printer for WSSC.

Item	Qty
Global Industrial™ Long Deck Mobile Scissor Lift with Oversized 63 x 32 Platform 1100 Lb.	1
Wood Based Composite Screw Extruder	1
16mm Ball Screw Assembly	1
700mm Guide Rails with stepper motor/carrage	1
1000mm Guide Rails with stepper motor/cariage	2
NEMA 34 Stepper Motor	1
Smoothieboard 5x	1
Low-Profile Mounted Sealed Steel Ball Bearing	2
Flange-Mounted Linear Ball Bearing (Top)	4
Flange-Mounted Linear Ball Bearing (Bottom)	4
Vibration-Damping Routing Clamp	8
Aluminium C-Channel (10')	1
Cut Angle Iron (36') and Cut Aluminum (4'x3')	1
Computer for printer control	1
24V Power supply	1
Linear Actuator	1
1/8" Steel Sheet (Nozzle mounting bracket)	1
1018 Steel Die	1
1018 Steel Nozzle	1
High pressure chemical Hose (4ft)	1
JIC fittings	2
3" Hinge	1
Fasteners	
Wiring	



### 3.2 Coupling of Printer and Screw Extruder

This work builds upon the screw extrusion method for wood AM developed by Thie [6], by incorporating a connection between the extruder and by making several enhancements to enable printing.

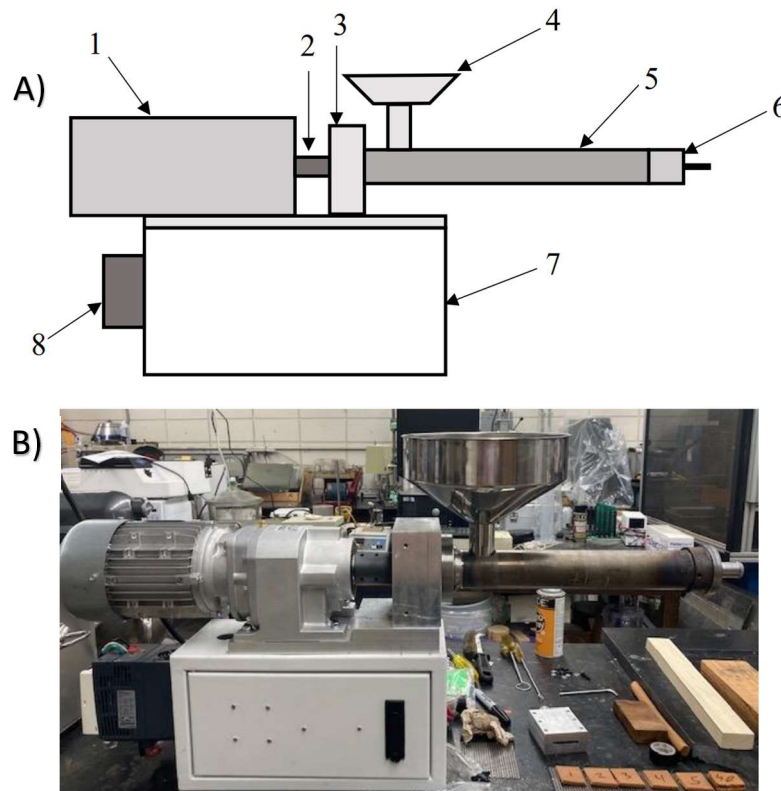


Figure 3-4: (A) Schematic representation of screw extruder system showing, (1) NORD motor, (2) shaft adapter, (3) bearing block, (4) hopper, (5) barrel, (6) die, (7) base, (8) VFD. Not Shown: screw. (B) Photograph of system [6].

To function as a 3D printer, it is necessary to couple the extruder to the frame/ gantry system. Two options for coupling exist: 1) mount the extruder directly to the linear guides of the frame, or, 2) connect the outlet of the extruder to the guides via a flexible hose to convey the material. The gearbox of the Nord electric motor only allows for mounting of the motor to be in a horizon position limiting the possible mounting positions. For this reason, a flexible hose was explored in this research.

Initial tests to understand the transportability of the material used a capillary rheometer (plunge extruder). A custom hose attachment was 3D printed and bolted to the die of the rheometer. The hose attachment is shown in Figure 3-6. This part was printed with a square infill pattern, 50% infill density, 2 mm walls, and 0.1 mm layer height. Attaching a hose to the capillary

rheometer showed the extrudate was still flexible and could be transported from the extruder die through a reinforced hose and undergo movement without jeopardizing any material properties.



Figure 3-5: (Left) Extrudate coming out of hose attachment bolted to die. (Middle) 300psi clear reinforced hose. (Right) extruded material leaving exit of reinforced hose.

It was previously determined that the pressure at the critical extrusion point, the point the composite begins to flow through the exit die, was 4.76 MPa (690 psi) [6], so a 6.89 MPa (1000 psi) high-pressure braided chemical hose was selected. Detailed specifications of the hose are shown in Appendix C. This heavy-duty hose was chosen because it is made from PTFE with a stainless-steel braid for more chemical resistance and better strength than other chemical hose. A 25.4 mm (7/8-in.) ID hose was chosen as it was the largest off-the-shelf high-pressure PTFE hose available and had a diameter close to the exit diameter of the already fabricated dies (Figure 3-7).



Figure 3-6: 25.4 mm ID high-pressure braided chemical hose [32].

Initially , a hose barb with hose clamps were used to secure the high-pressure braided hose to the die but this method was not strong enough to keep the hose attached. The hose would become detached as shown in Figure 3-7.

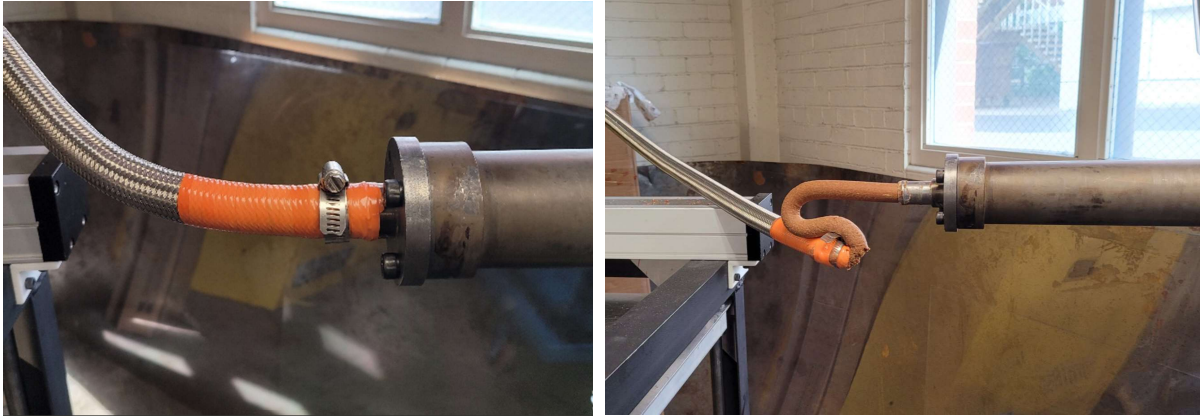


Figure 3-7: (Left) Hose clamp with high-pressure hose. (Right) Failed connection.

To overcome this, new connectors were used to secure the hose to the die. Joint Industrial Council (JIC) fittings shown in Figure 3-8 were chosen for ease of manufacturing purposes of the new die. Detailed specifications of the JIC fittings are show in Appendix D.

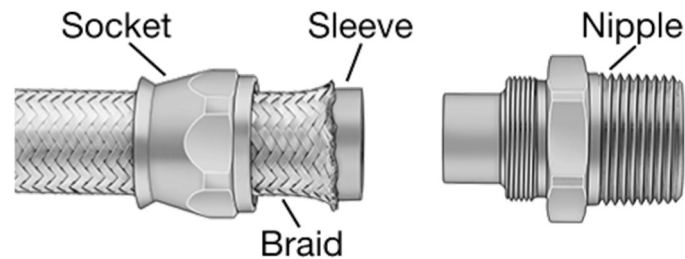


Figure 3-8: Assembly of hose and fitting [32].

Changes to the die were necessary to accommodate the new fittings for the high-pressure hose. A new 1-5/16" – 12 threaded die was designed and manufactured out of 1018 steel. The new die also includes a port for a ZHYQ N70 pressure sensor to measure pressure during extrusion. Figure 3-9 shows the die, pressure gauge, fitting, and hose fully assembled. Detail drawings for the threaded die are show in Appendix E.



*Figure 3-9: Connection to screw extruder.*

After several extrusion attempts it was found that the connection inside the fitting was a critical failure point due to over-bending of the hose. The failure of the connection is shown in Figure 3-10. To overcome this problem a stiffener was added over the socket and hose for strain relief. Figure 3-11 shows the stiffener consisting of a 38.1 mm ID, 100 mm long aluminum tube, 31.75 mm heat shrink and gasket between the hose and the tube.



*Figure 3-10: Failed Connection*



*Figure 3-11: Fully assembled hose fitting with stiffener. Gasket not shown.*

The first iteration for connection to the 3D printers linear guide was accomplished using a custom bracket 3D printed from PLA material on a Sindoh 3D-WOX 2 3D printer. This part was printed with a square infill pattern, 50% infill density, 2 mm walls, and 0.1 mm layer height. Figure 3-12 shows the X-axis liner guide mount with the bracket attached to it with the high-pressure braided hose secured inside of it.



*Figure 3-12: First iteration of printer connection.*

The mounting position of the extruder relative to the 3D printer required a minimum of 1079.5 mm of high-pressure braided hose. This length of hose was necessary to allow for the 228.6 mm (9 in.) minimum bend radius of the hose while still allowing the print nozzle to reach all corners of the print bed. Figure 3-13 shows the extruder to nozzle height relationship and extruder position with the print bed.

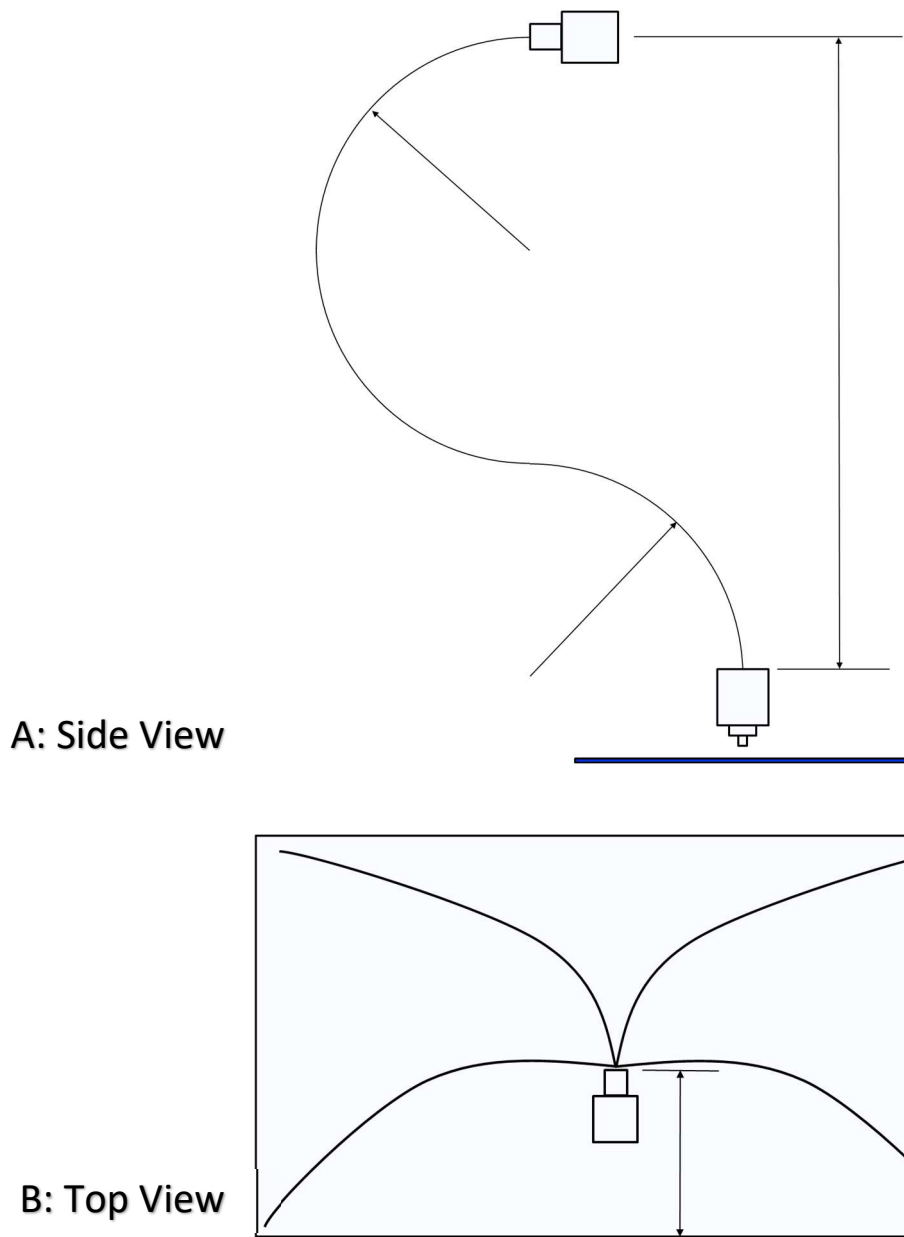


Figure 3-13: (A) Extruder die must be mounted at least 685.8 mm (27 in) above nozzle. (B) Extruder nozzle must be mounted in the center of the Y-axis and 228.6 mm (9 in) from edge.

The final modification made to the 3D printer frame was to the height of the frame. The initial height of the printer frame was too tall to accommodate the preexisting tables. 304.8 mm (12 in.) was removed from the Z-axis height and was reassembled. Figure 3-14 shows the extruder and 3D printer frame set up before shortening Z-axis.



*Figure 3-14: 3D printer and extruder height problem.*

To prevent the WSSC from curing inside of the high-pressure braided hose, an inert material was fed into the extruder. The inert material pushes the WSSC out of the extruder and hose after each run. It was found that a commercially available mixture of cracked corn and whole wheat, known as scratch grain, mixed with water worked well for this purpose. Four cups of scratch grain was mixed with one cup water in the food processor to create a consistency similar to that of the WSSC. The scratch grain fully replaced all of the remaining wood-sodium silicate left in the barrel, die, and hose. The region with both WSSC and scratch grain can neither be left inside the extruder nor used for printing. This region can be seen in Figure 3-15 and shows a minimal amount of waste was produced at the transition zone between the two materials.



*Figure 3-15: Transition zone between the sodium silicate and scratch grains.*

### 3.3 Nozzle Design

The overall goal of this project was to print building wall sections with geometric reinforcement of solid sections, so it was determined that an extrusion with a rectangular cross-section would best accomplish this. A nozzle was designed to alter the shape of the material being extruded from a circular to rectangular cross section. The rectangular shape shown in Figure 3-16 for the nozzle exit was chosen because when stacked it would create a 2"x4" timber or a panel when laid next to one another.



Figure 3-16 Example of layered extrudate.

The exit of the nozzles cross sectional area was determined by the 22.2 mm (7/8 in.) diameter die and hose combination. All the printed nozzles were 3D printed using a Sindoh 3DWOX printer with Sindoh PLA. This nozzle was printed with a square infill pattern, 15% infill density, 2 mm walls, and 0.1 mm layer height. The nozzles first iterations (V1) layer height was 2.8 mm, and a width of 73.7 mm. The nozzle's first iterations can be seen in Figure 3-17. These designs allowed the hose to be placed inside or over top of the nozzle connection.

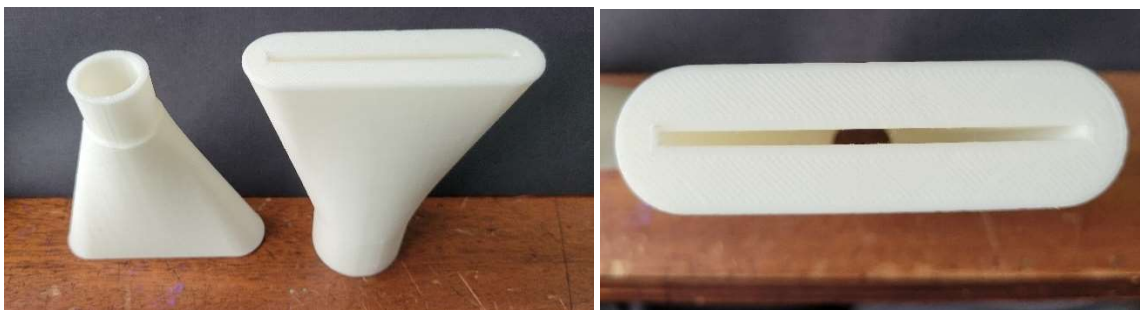


Figure 3-17: (Top) Nozzle V1 with two hose connection types. (Bottom) Exit of nozzle.

It was found that the hose placed over the nozzle worked best. Figure 3-18 shows the first nozzle secured to the clear nylon hose with 25.4 mm (1 in.) hose clamps.





*Figure 3-18: Nozzle, hose, and die attached together with hose clamps.*

Initial tests proved the material could be transported through the hose and begin to be deformed, however, full extrusion did not occur before critical failure of the nozzle. Figure 3-4 shows the WSSC filled inside of the failed nozzle. Failure occurred between print layers.



*Figure 3-19: (Left) Nozzle filled with material at failure. (Right) Deformed material at exit of nozzle.*

The second iteration (V2) of the nozzle implemented a two-piece design. This had three benefits. First, by reorienting the print direction of the nozzle halves, the interlayer forces during extrusion were changed from tensile to compressive. Second, this design was easy to clean any remaining WSSC. Third, this design allowed the nozzle to be machined from metal in later iterations if needed. A barb was added to the nozzle to better secure the hose. Figure 3-5 shows the nozzle V2 in two pieces and assembled. The exit of the nozzle was changed to have a height of 6.4 mm and width of 45 mm. This was done to reduce the deformation of the extrudate inside the nozzle compared to V1 while retaining dimensions suitable for panel construction. The V2 nozzle was printed in PLA with a square infill pattern, 60% infill density, 2 mm walls, and 0.1 mm layer height.



Figure 3-20: (Top) V2 nozzle halves. (Bottom) Exit of nozzle.

The two halves of the V2 nozzle were secured together using four, 25 mm M5X8 bolts. During extrusion it was found that the internal pressure deformed the polymer nozzle, so a c-clamp with small wood pieces was placed around the it to stop the two halves from separating. Figure 3-21 shows the WSSC successfully being deformed and extruding from the nozzle. After several higher-pressure extrusions, the V2 nozzle ultimately failed at the hose connection feature shown in Figure 3-22.

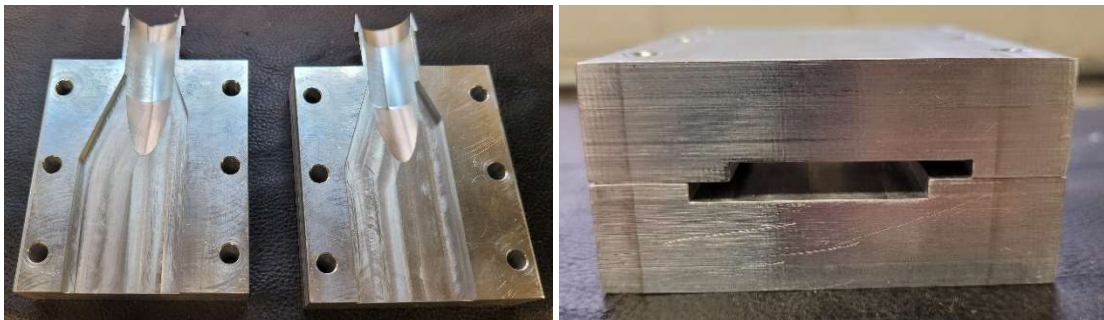


Figure 3-21: Successful rectangular extrusion.



*Figure 3-22: Failed V2 nozzle.*

A third nozzle (V3) was machined out of 6061 aluminum and was designed to produce extrudate that could lock together with a rabbit joint. The rabbit joint was intended to help the mechanical connection between horizontal layers. Figure 3-8 shows the two halves of the V3 nozzle and the exit shape of the extrudate. The two halves of the nozzle were secured together with four, 50.8 mm  $\frac{1}{4}$ "-28 bolts.



*Figure 3-23: V3 aluminum nozzle with rabbit joint.*

The V3 nozzle caused severe surface defects (shark skin) on the extrudate and was later machined out to a rectangular profile. The nozzle has a layer height of 6.4 mm and width of 45 mm.

The V3 nozzle was secured to the high-pressure braided hose using a 25.4 mm (1 in.) hose clamp. Less than 610 mm of material could be extruded at a time before the nozzle became detached from the hose. Figure 3-24 shows the V3 nozzle successfully extruding the rectangular shape.



Figure 3-24: V3 nozzle with rectangular extrudate.

The V4 nozzle used the same extrudate exit geometry as the V2 nozzle but was designed and manufactured from 6061 aluminum with 1-5/16" -12 threads for the JIC fitting. Alignment pins were used to properly align threads. The V4 nozzle is shown in Figure 3-25 attached to the high-pressure hose with the JIC fitting.

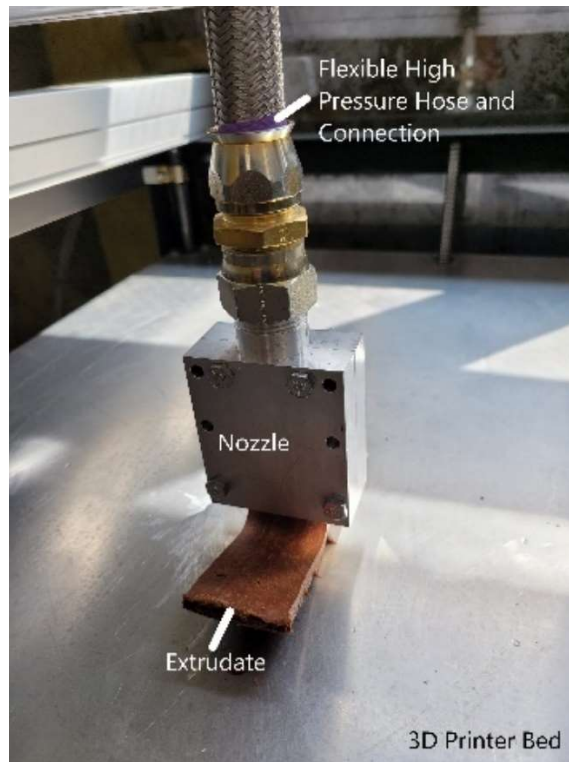


Figure 3-25: V4 nozzle with JIC fitting.

The V4 nozzle allowed for longer extrusion times. Because of the longer extrusion times, a chemical reaction was observed between the nozzle and WSSC causing the material to cure inside the nozzle. Figure 3-26 shows the WSSC stuck inside of the nozzle and a rough residue left behind after removal. This curing caused irregular flow inside of the nozzle and after 1065 mm of extrusion, shark skinning appeared. Figure 3-27 shows the extrudate shark skinning after the third section.



Figure 3-26: (Left) WSSC cured inside nozzle. (Right) Residue left behind after cleaning.

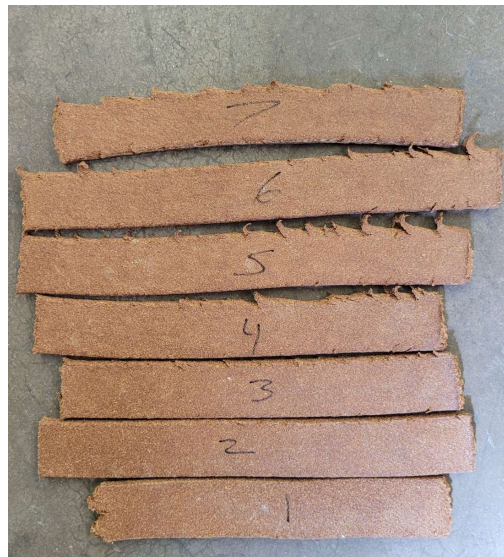


Figure 3-27: Extruded WSSC with shark skin.

The V5 nozzle was machined out of 1018 steel, the same material as the die. This nozzle was still constructed in two halves but for ease of machining, the threads were kept to a single half. The threaded and non-threaded halves of the V5 nozzle are seen in Figure 3-28. A detailed drawing of the V5 nozzle is shown in Appendix F.



*Figure 3-28: V5 nozzle made of 1018 steel.*

### 3.4 Cooling System

Compressing the WSSC inside the barrel generates a significant amount of heat due to friction. The sodium silicate is a thermoset resin and will begin to cure inside the extruder's barrel and continue curing during transportation to the print bed if the temperature is too high. The characteristics of the extrudate change drastically as the temperature of the extruder barrel increases, becoming much more brittle and unable to flex once extruded. The difference in the extrudate's physical appearance can be seen in Figure 3-29. The extrudate at the top of the figure was done first with the barrel at room temperature,  $\sim 22^{\circ}\text{C}$ , while the bottom extrudate was sampled once the extruder barrel reached  $52.5^{\circ}\text{C}$ .



Figure 3-29: (Top) Extrudate at room temp. (Bottom) Extrudate at  $52.5^{\circ}\text{C}$ .

As seen in Figure 3-30, a cooling system was designed to maintain a constant barrel temperature during long extrusions. A 76.2 mm (3 in.) diameter steel pipe was fitted over the extruder barrel and fitted with 6.4 mm (0.25 in.) inlet and outlet fittings to function as a counter-flow heat exchanger. An aquarium pump was used to circulate room temperature water from a bucket at 272.7 LPH (60 GPH) through a 6.35 mm (0.25 in) clear hose. Figure 3-30 shows the cooling system fitted over the extruder barrel.

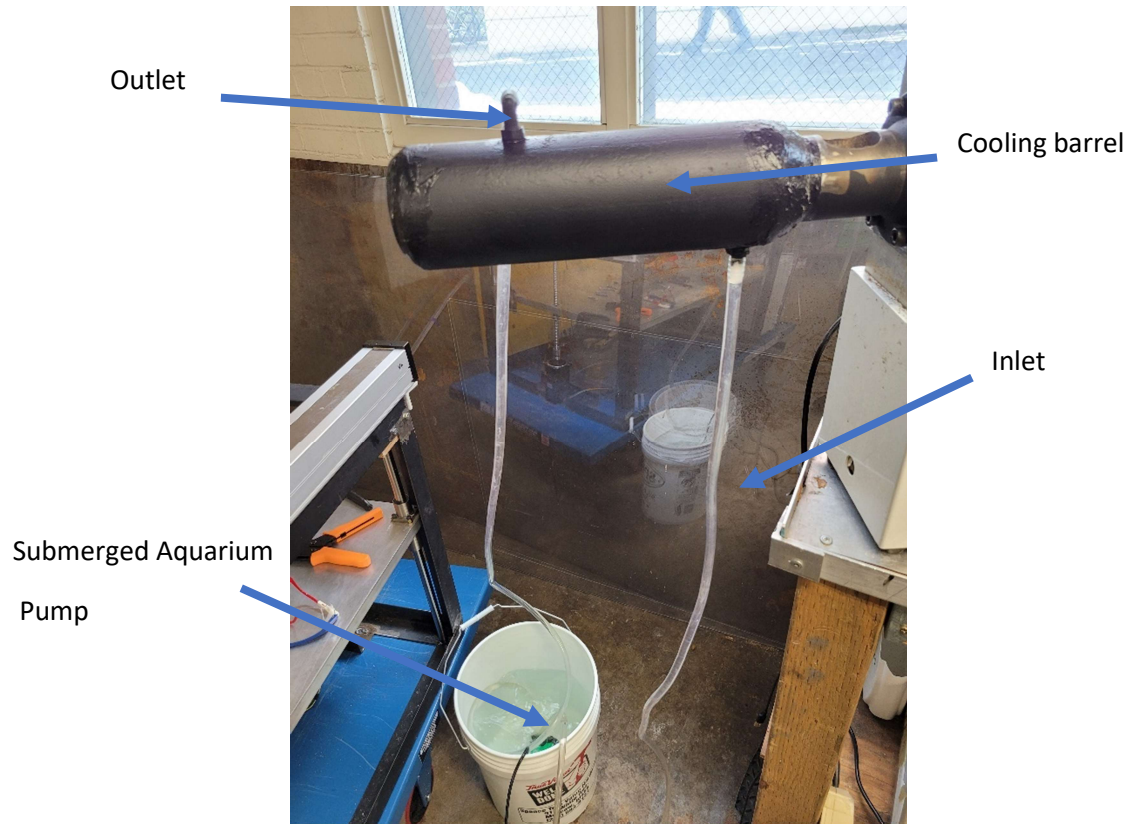


Figure 3-30: Cooling system

The addition of the cooling system reduces the steady-state temperature of 52.5°C seen at the extruders barrel to 23.1°C. Figure 3-31 shows thermal images taken with an infrared camera of the extruder barrel with and without cooling.

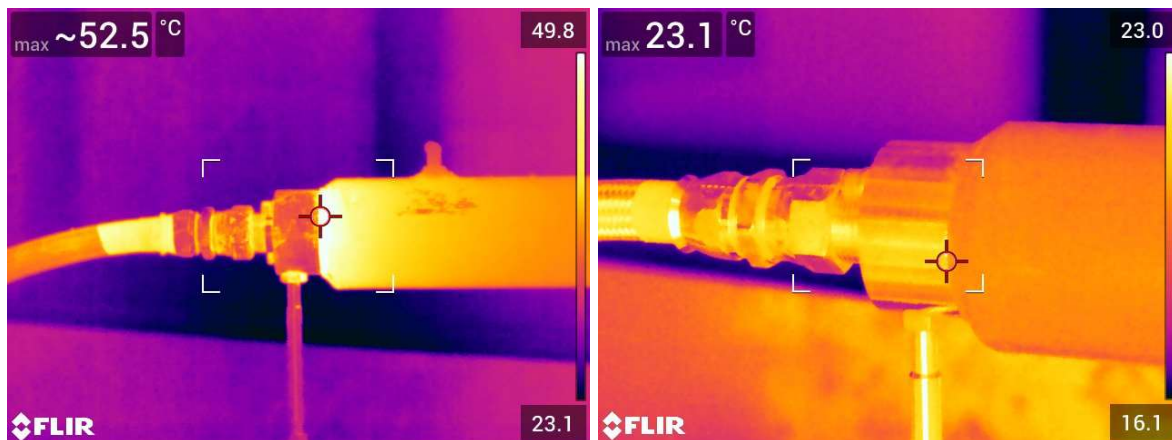


Figure 3-31: (Left) No cooling. (Right) With cooling.



### 3.5 Nozzle Rotation

The design of the nozzle does not allow for printing in both the X and Y directions without being rotated 90 degrees about the extrusion axis. To allow the nozzle to rotate, a bracket with a linear actuator was designed. The nozzle was connected to the bracket with a 76.2 mm (3 in.) door hinge. Figure 3-32 shows a schematic of the nozzle rotation. Detailed drawings of the nozzle bracket are shown in Appendix G.

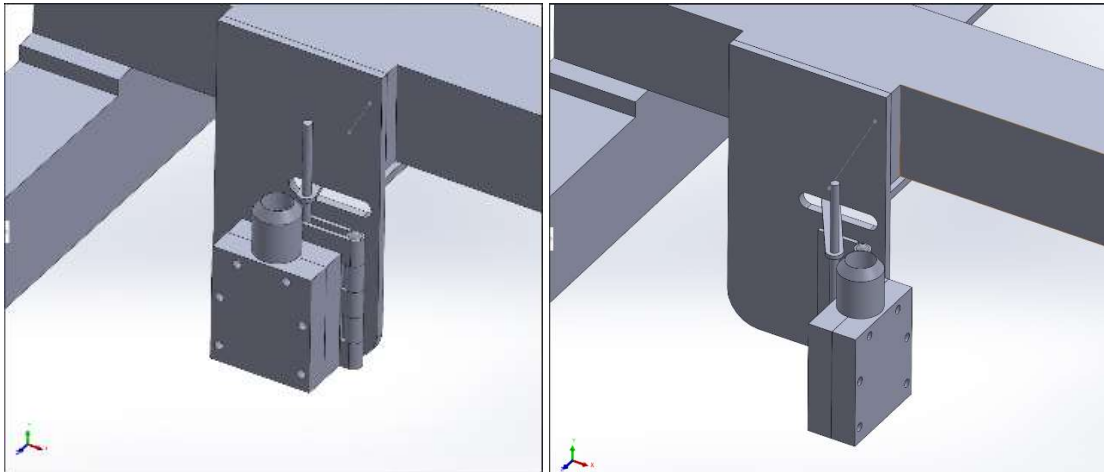


Figure 3-32: (Left) Nozzle in home (0-degree) position. (Right) Nozzle in 90-degree position.

The first linear actuator used was a linear actuator with a 63 N holding force. The high pressures seen inside of the hose during printing caused the hoses to be much less flexible, and it was discovered that the 63 N actuator was not strong enough to rotate the nozzle. It was replaced by a linear actuator with a 957 N holding force. Figure 3-33 shows the two linear actuators.



*Figure 3-33: (Left) 63 N holding force linear actuator. (Right) 957 N holding force linear actuator.*

Attaching the larger linear actuator required modifications to the mounting bracket. The mounting points of the linear actuator were extended back to make room for the larger actuator. Gussets were also added to the bracket to make it more ridged and durable for the higher holding force. Figure 3-34 shows the welded gussets in place with the linear actuator in the home position.



*Figure 3-34: Added gussets to bracket to support larger actuator.*

The linear actuator was attached to the nozzle by two M5 bolts. Figure 3-35 shows the linear actuator attached to the nozzle in the 90-degree position.



*Figure 3-35: 957 N linear actuator with nozzle in 90-degree position.*

## Chapter 4: Programming and Controls

The 3D printer is controlled from a desktop computer via the SmoothieBoard and PronterFace software interface. SmoothieBoard is an open-source hardware mill, 3D printer, or laser controller designed to run Smoothieware firmware. This section details the connection and programming of the SmoothieBoard.

### 4.1 SmoothieBoard Configuration

The SmoothieBoard is connected to the desktop through a high-speed USB to ethernet cable. A 24 V power supply is connected to the SmoothieBoard to power the connected X-, Y-, and Z-axis stepper motors and the linear actuators DC motor for the rotating nozzle. Figure 4-1 shows the control system layout for the 3D printer.

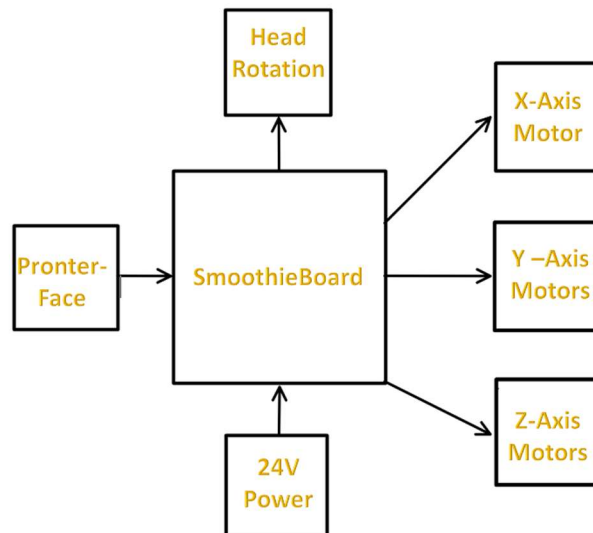


Figure 4-1: 3D printer control system layout.

The pin configuration of the SmoothieBoard can be seen in Figure 4-2. The 24V power supply and ground are connected to the main power input, VBB IN and GND. The X-axis uses a single stepper motor connected to the first stepper driver (M1). The Y and Z axis both require two stepper motors each. The smoothie drivers are unable to supply a current more than 2A, meaning each motor requires its own driver. Having three axes, two of which need two drivers, a total of five drivers were needed. To ensure the two motors with a single axis stayed in sync with one another the drivers are wired together or slaved to each other. This means one driver controls the other. The Y-axis uses stepper driver M2 with M4 slaved through pin EN2 to pin EN4, pin ST2 to pin ST4, and pin DIR2 to pin DIR4. The Z-axis uses stepper driver M3 with M5 slaved through pin EN3 to pin EN5, pin

ST3 to pin ST5, and pin DIR3 to pin DIR5. The DC motor moving the linear actuator is connected to the SmoothieBoards small mosfets, Q8 and Q9. The jumpers were set to allow the mosfets to switch the power from the VBB.

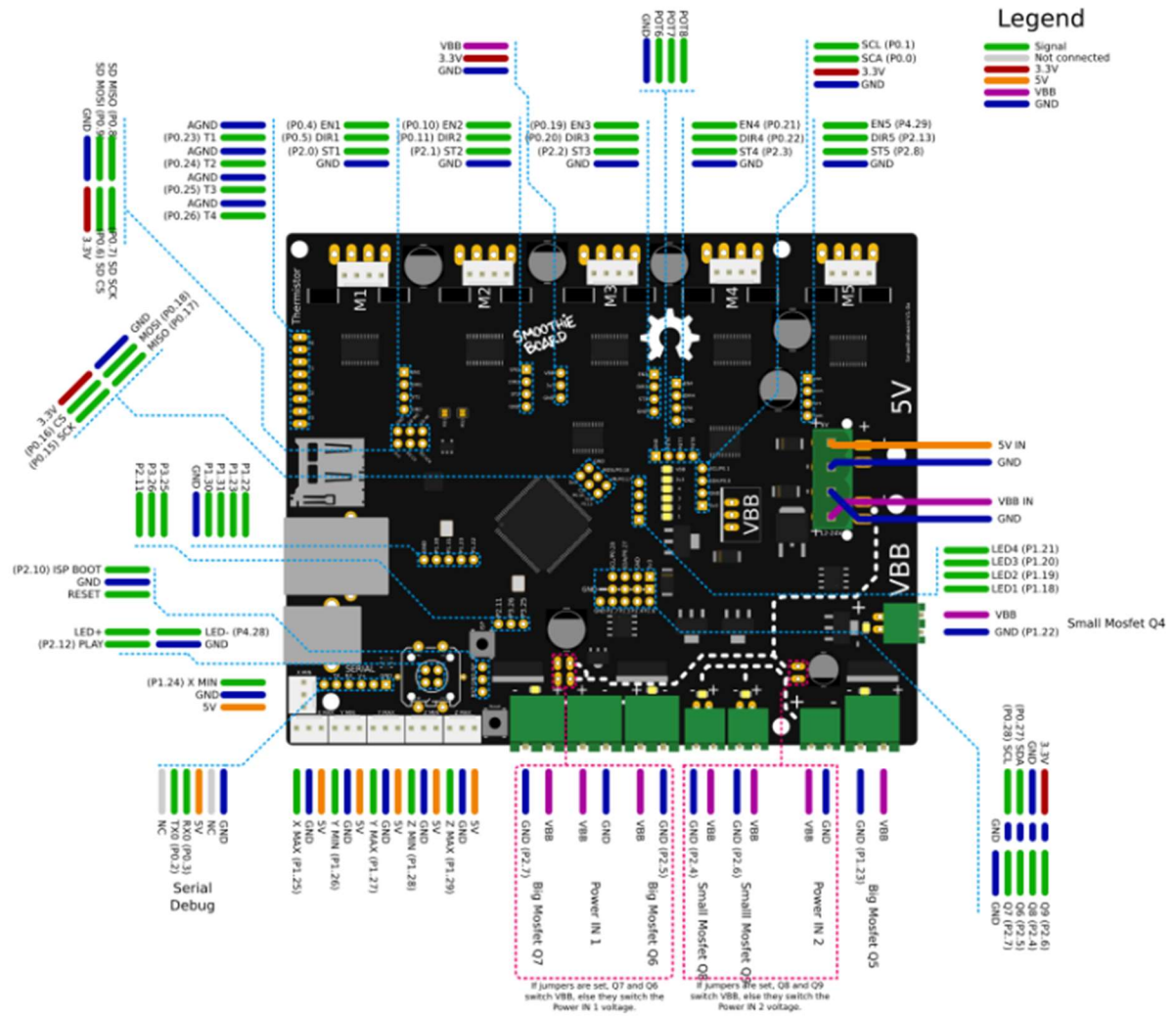


Figure 4-2: SmoothieBoard pin configuration.

## 4.2 Smoothieware Configuration

The Smoothie firmware is configured by editing a text document located on its micro-SD-card. The configuration file must be named “config” for the SmoothieBoard to be able read the file. An open-source default config file for 3D printing was downloaded from Smoothieware and edited as needed. The full config file can be seen in Appendix H. The basic motor configurations default feed rate is 3000 mm/min and default seek rate is 2000mm/min. The arm solution configurations translate millimeter positions into stepper positions. The steps per mm for each stepper motor was calculated using the equation

$$\text{Steps per mm} = \frac{\text{Stepper Motor Steps}}{(\text{Micro Steps} * \text{Lead Distance})} \quad (3)$$

Where stepper motor steps are number of steps per revolution, the micro steps are the drivers microstepping abilities, and lead distance is the mm traveled per revolution of the screw. Each stepper motor was assigned either an alpha, beta, or gamma signal. The X-axis stepper motor (alpha) was set to 640 steps/mm. The Y-axis (beta) was set to 640 steps/mm and the Z-axis (gamma) was set to 400 steps/mm.

Acceleration and maximum speed values are all pulled from stepper motor data sheets. The hard wiring of the stepper motors mentioned in Chapter 4.1 were entered into the Stepper module configurations.

### 4.3 PronterFace G-code

In order for the 3D printer to execute anything it has to be given a command. PronterFace is a simple graphical user interface that allows the user to monitor and control the printer from a USB-connected computer. Once connected, Pronterface can directly move the stepper motors, control head rotation, and send G-code commands to the printer via a file or console window. Figure 4-3 shows the Pronterface user window and the different methods for entering commands to the different components.

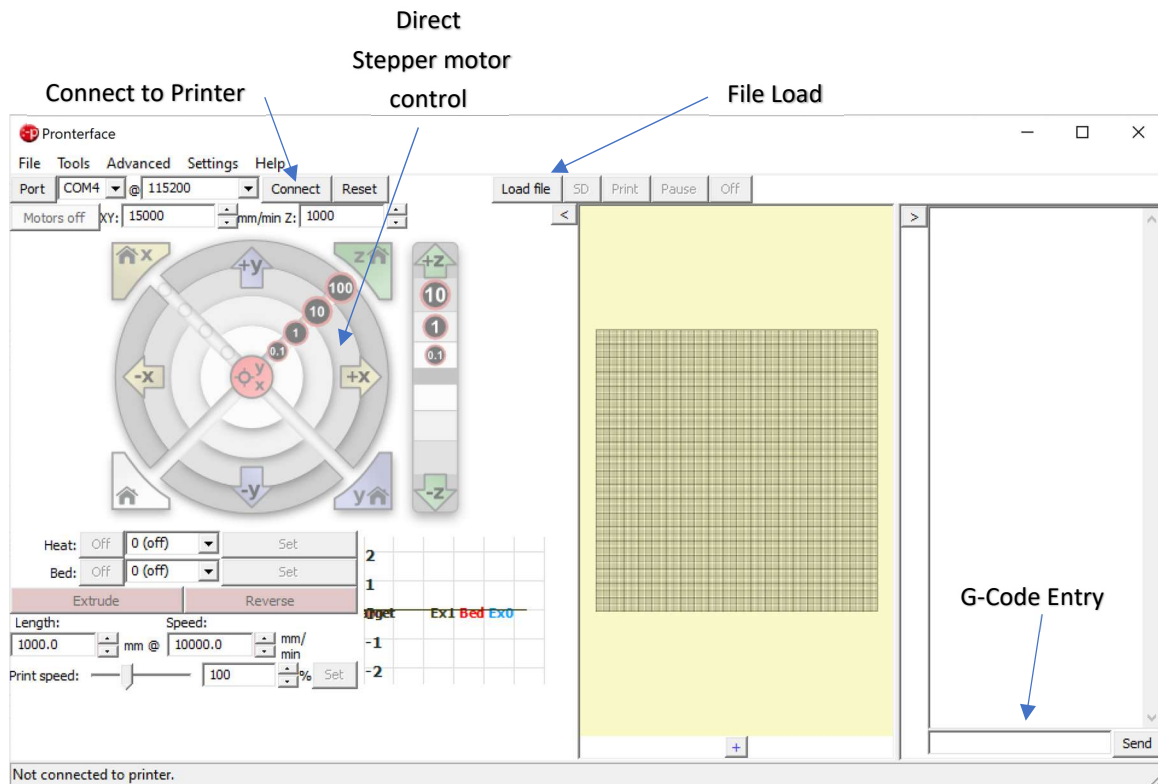


Figure 4-3: PronterFace user window.

Four G-code text files were created to run on the 3D printer for WSSC: 1) Printer Check, 2) Panel, 3) Studded Wall, and 4) 2" x 4". Figure 4-4 shows the "Printer Check" G-code file used to calibrate the printer before starting each print. The G-code for each of the remaining prints can be seen in detail in Appendix I, J, K.

```

Printer Check - Notepad
File Edit Format View Help
G0 X0 Y0 Z0 F2000

G0 X475 Y900 Z-825 F2000

G4 S5

G0 X237.5 Y450 Z0 F2000

G4 S5

G0 Z-22 F2000

G0 X0 Y0 Z0

```

Figure 4-4: Printer Check G-code

Once the printer is connected to the computer, the “Connect” button will change to “Disconnect” and a message in the read-out window will appear stating the Printer is now online.

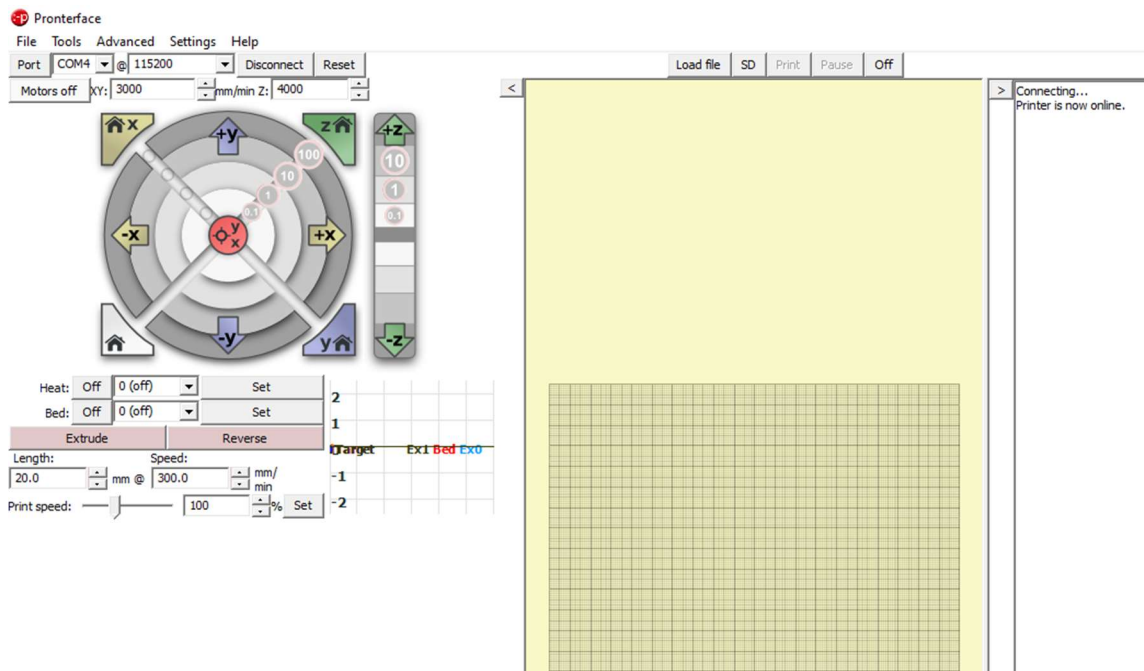


Figure 4-5: Printer connected to Pronterface.

Now that the printer is connect to the computer a G-code file will be loaded for it to run. Navigate to the “Load File” button and select “Load SD File.” Figure 4-6 shows the window that appears to select the desired .txt document to run a print.



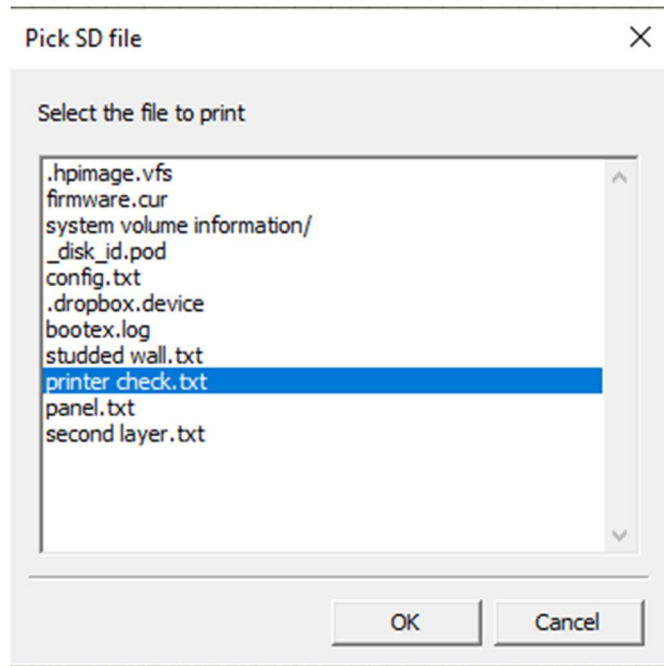


Figure 4-6: G-code selection window.

Once the desired .txt document is selected and ok is pressed, the print begins. A notification in the message window will appear showing the time the print started. Figure 4-7 shows the running print file.

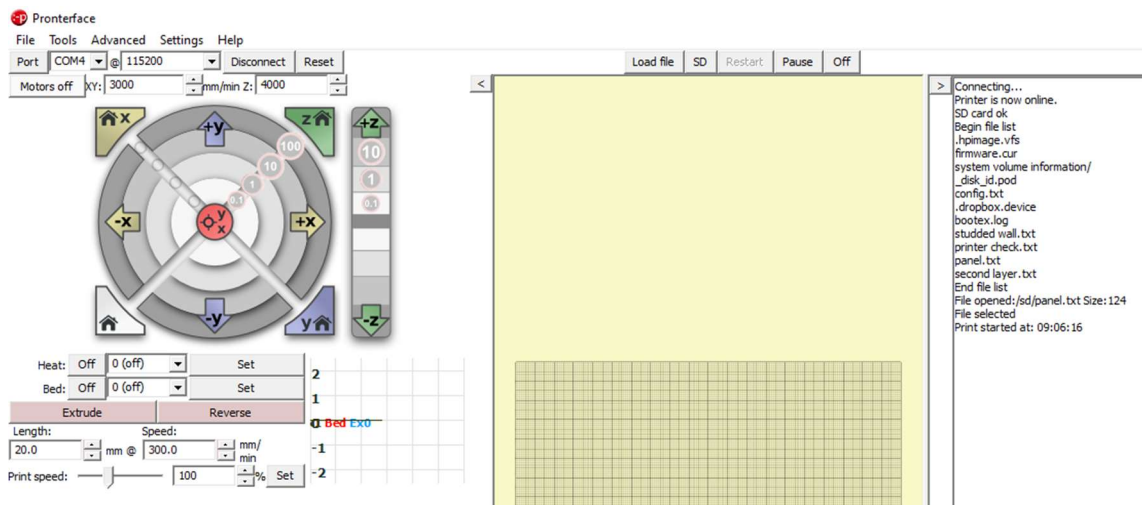


Figure 4-7: Running print file.

## Chapter 5: Printing Parameters

### 5.1 Wood and Resin Mixture

Wood waste from Plummer Forest Products (Post Falls, Idaho) was used for the wood flour in this research. It was sieved to a primary element size of less than 40 mesh (< 40) with a sifter shown in Figure 5-1, where 40 mesh is a standard US mesh that has a sieve size of 0.425 mm. The moisture content of the wood fiber was measured using a HB43-S Halogen Moisture Analyzer from Mettler Toledo, Columbus OH. The moisture content ranged between 5.8% and 7%. The primary binder used was sodium silicate ( $\text{Na}_2\text{O}_3\text{Si}$ ) from Thermo Fisher Scientific (Carlsbad, CA). Sodium silicate is a water-soluble thermoset resin. The sodium silicate was premixed with water to form a solution at a weight ratio of 37% sodium silicate to 63% water from the manufacturer. The weight ratio of wood to sodium silicate was evaluated at different ratios between 40:60 and 60:40. To obtain a 50:50 weight ratio, 2.7 g of the sodium silicate solution was added for every 1 g of wood flour.



*Figure 5-1: Less than 40 mesh wood flour being sieved.*

To make a batch of WSSC for printing, sodium silicate solution and wood flour was first hand-mixed to reduce dust and heat created during the second mixing step. The mixture was then placed in a high torque food processor for approximately 10 s to fully combine. Figure 5-2 shows the WSSC inside the food processor before being mixed. Batches using between 50 g and 200 g of wood flour were mixed at a time to prevent unwanted curing while the mixture waited to be fed into the extruder. One-hundred-gram wood-flour batches were the primary batch size.



*Figure 5-2: WSSC placed in food processor.*

The addition of tap water at different percentages of the overall weight between 1% and 5% was also assessed to lower viscosity and improve flow. Figure 5-3 shows a 50:50 ratio mixture with 1% additional water added to it.



*Figure 5-3: Mixture with added water on parchment paper*

Binder jetting techniques were evaluated by spreading a thin layer of wood flour across a piece of parchment paper and pouring a small stream of sodium silicate solution over the top (Figure 5-4).



Figure 5-4: (Left) Pour-over mixing before curing. (Right) After curing.

After mixing, storage of the WSSC for 24 hours at different temperatures was explored. Figure 5-5 shows the WSSC placed inside a freezer bag with all of the air removed and sealed. The weight of the mixture was taken before and after the 24 hours.



Figure 5-5: (Left) Stored at room temperature. (Right) Stored in stand-up freezer.

The mixing of the material inside of the extruder barrel was tested using green gel food coloring. The food coloring was placed along a section of material before being placed inside of the extruder's barrel (Figure 5-6).



*Figure 5-6: Green food coloring placed on top of material.*

## 5.2 Extruder Settings

All extrusions were done at room temperature (21°C – 23°C). The extruder's 745.7 W (1 hp) NORD AC Gearmotor 230/460 has an ideal torque of 178.0 N-m. The maximum speed of this motor is 40 RPM, and it uses a gear ratio of 43.2:1. An Altivar 12 variable frequency drive (VFD) was used to control the motor's speed. All extrusions and prints were done at the maximum motor speed of 40 RPM. Compression and non-compression screws were examined inside the extruder. A zero-compression screw was found to work best.



*Figure 5-7: Zero-compression and compression screws.*

### 5.3 Curing Characteristics

How the extruded samples are dried and cured was varied to test if the curing method influences the final sample. The curing temperature was varied to evaluate its effects on the WSSC's density, water resistance, fire resistance, and interlayer adhesion. The oven temperatures evaluated were room temperature (20°C), 60°C, and 105°C. The curing time was 48 hours for samples cured in the oven and eleven days for samples cured at room temperature. All samples had a 50:50 wood to sodium silicate weight ratio.

Five samples from each sample set were cut to approximately 50 mm x 50 mm pieces for the water soak test. Measurements of the length, width, thickness, and weight were taken before and after soaking samples in water for 24 hours to determine the change in density. The percentage (%) change in thickness for water-swollen condition was then compared to original dimensions. The percent (%) change in water absorption (weight gain) was also recorded. Figure 5-8 shows a picture of five room temperature cured samples after immediately being placed into the water.

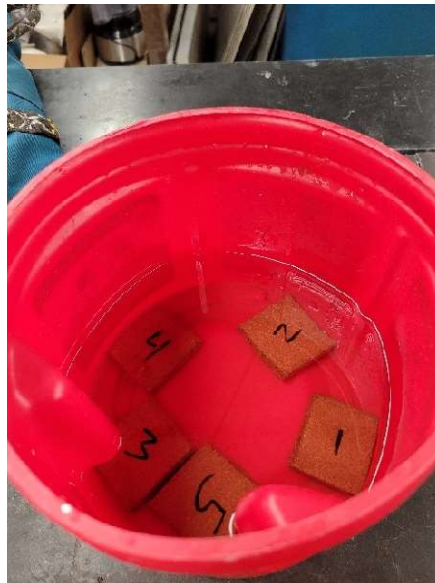


Figure 5-8: WSSC water soak test.

### 5.4 Bed Adhesion and Removal

In order to successfully deposit and remove printed material from the print bed, the nozzle travel speed, nozzle/printer-bed-height relationship, and bed surfaces were assessed. Figure 5-9 shows the nozzle and print bed height,  $H_B$ , and nozzle head velocity,  $V_N$ . Extruded WSSC does not adhere to the aluminum print bed if deposited as free extrudate (Figure 5-10). The extrudate adheres, starts to cure, and becomes extremely difficult to remove from the aluminum print bed if the print is initially held in place by hand. The length of time it takes to 3D print a part is much greater than the time it takes the resin to start curing. The resin begins to cure ten minutes after mixing and larger prints can take multiple hours. This resulted in the part adhering to the bed too strongly and being damaged during removal (Figure 5-11)

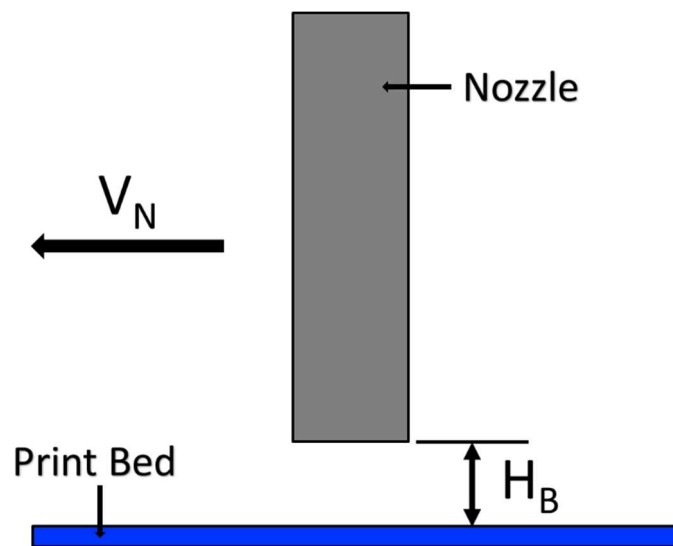


Figure 5-9: Nozzle/Print-Bed relationship.



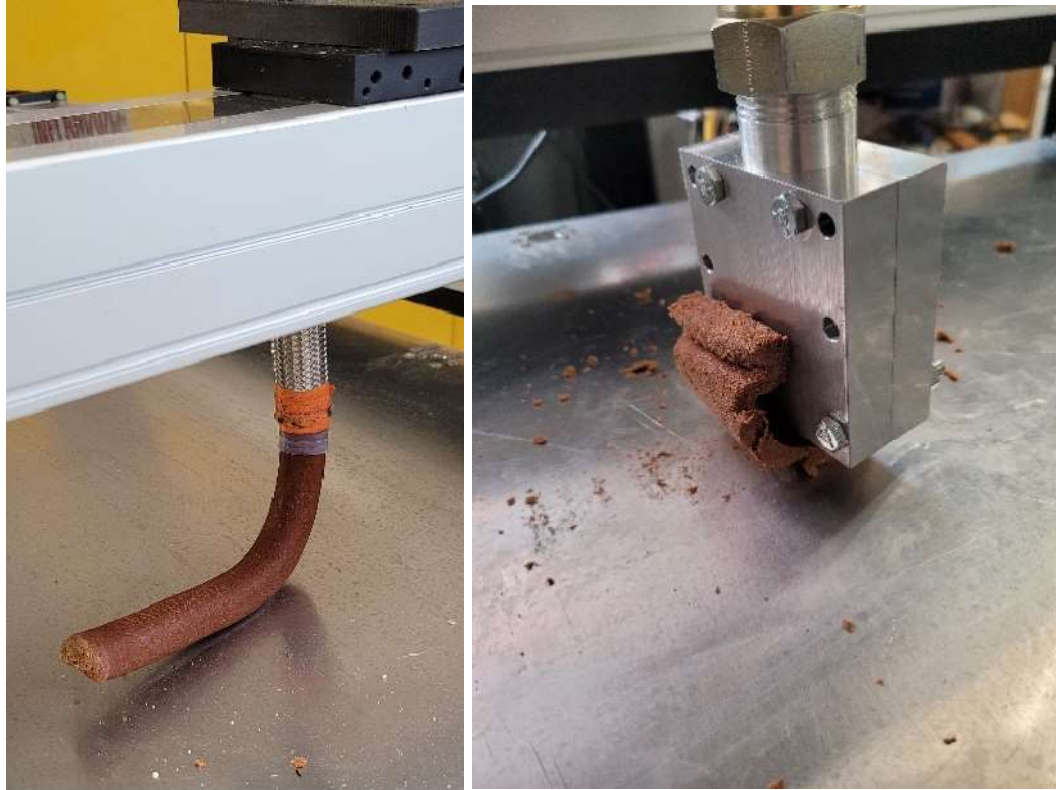


Figure 5-10: (Left) Extrudate freely coming out as round extrudate. (Right) Rectangular extrudate curling up from bed.



Figure 5-11: Printed material held at beginning of print with second layer.

The WSSC left behind after removing the printed parts was extremely difficult to remove from the bed. Figure 5-12 shows the before and after addition of blue painters tape to the surface allowing for the extrudate to be pressed onto the surface without it adhering to the print bed. This allowed for it to be easily removed and transported to an oven for curing.



*Figure 5-12: (Left) Printed Extrudate left on aluminum bed. (Right) Blue painters tape applied to bed surface.*

### 5.5 Interlayer Adhesion

One of the key factors of AM is the interlayer adhesion of the printed material. Interlayer adhesion can dictate the overall strength of the printed structure. Chemical and mechanical adhesion between the extrudate was assessed. Vertical and horizontal layering of the material were assessed.

To first understand how the extrudate adhered with itself, a 50:50 ratio batch was extruded through the 22.2 mm (7/8 in.) diameter die and broken into pieces between 50 mm and 100 mm long, as show in Figure 5-13. The two stacks each contain four broken pieces of various length. The stack on the left was pressed into a ball as tightly as possible by hand while the right stack was pressed together vertically, also by hand, until major surface fractures were present. Figure 5-14 shows the two stacks in their respective pressed configurations.



Figure 5-13: (Top) Extruded Rod. (Bottom) Rods broken into pieces.



Figure 5-14: (Left) Pressed ball extrudate. (Right) Vertically pressed extrudate.

Adhering the extruded material vertically was first assessed using both chemical and mechanical methods seen in Table 5-1. Failure of the interlayer adhesion is defined by any separation of the layers at the boundary layer. The added materials were applied to the surface of the extrudate using either a hand spray bottle, paint sprayer, paintbrush, or was poured over and spread with finger. Both surfaces being adhered together had material added to it. All samples were cured at 60°C for 24 hrs. The pressure added to the layers before curing was done by hand to the point before surface deformation was present. All sample types were dried with and without pressure during the curing. The pressure during curing was done with two, 1.14 kg (2.5 lb.) fire bricks with a mesh screen between material stacked on top.

Table 5-1: Interlayer adhesion properties

Pressure Before Curing	Added Material	Result
No	N/A	Fail
No	Liquid Sodium Silicate	Fail
Yes	N/A	Fail
Yes	Liquid Sodium Silicate	Fail
Yes	Water	Fail
Yes	Solid Sodium Silicate	Fail
Yes	Solid Sodium Silicate and Water	Fail
Yes	80% Alcohol	Fail
Yes	91% Alcohol	Fail
Yes	Disinfectant	Fail
Yes	Ace Cleaner	Fail
Yes	Dawn Soap	Fail
Yes	Damn Soap and Water	Fail
Yes	Foamy soap and water	Fail
Yes	Fast Orange Cleaner	Fail
No	Aluminum Oxide Powder	Fail

Four (1.75 in. by 6 in.) samples were stacked on top of one another with 0.15 Mpa (21.4 psi) of pressure for five minutes before being placed in the oven for 24 hrs. at 60 °C with pressure.

Two panels consisting of five 305 mm long layers placed side-by-side to one another was constructed. The panels were oriented 90-degrees to one another and layered to create a cross pattern shown in Figure 5-15.

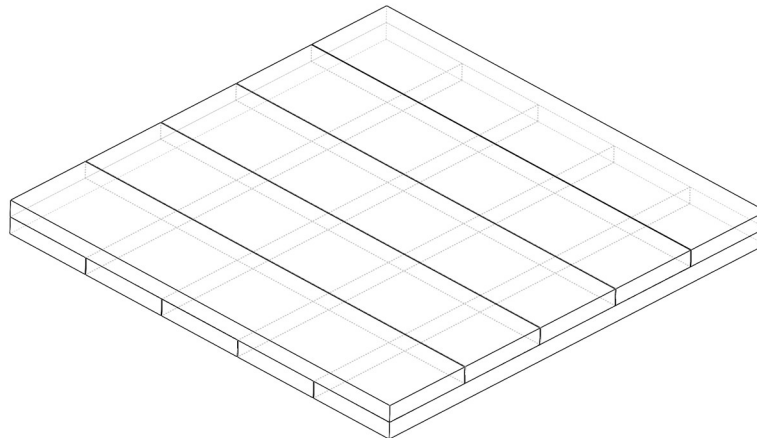


Figure 5-15: 90-degree layer orientation.

The nozzle's relative location to the previous layer and the bonding of the interlayers was assessed. The two bonding directions assessed were the vertical and horizontal print directions. Figure 5-16 shows the key variables looked at when assessing the nozzle position and interlayer bonding.  $V_N$  is the nozzle head velocity,  $H_L$  is the height between layers, and  $D_L$  is the distance between the center of each printed layer. Once samples were printed and cured they were broken by hand applying force to either side of the layer boundary to visually observe boundary failure.

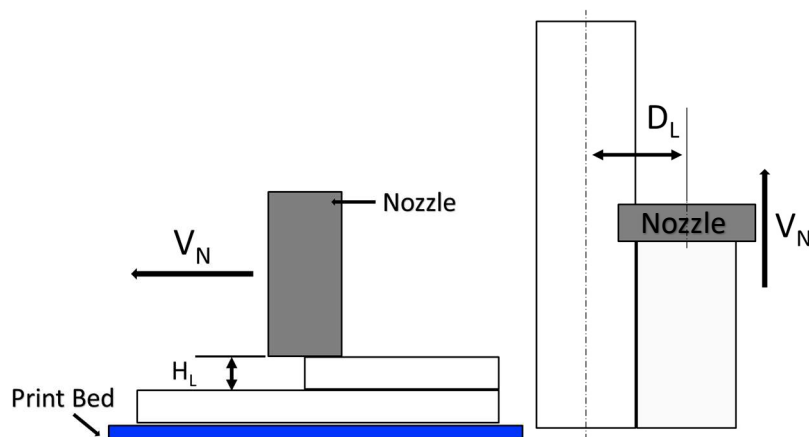


Figure 5-16: (Left) Vertical layering. (Right) Horizontal Layering

## Chapter 6: Results

### 6.1 3D Printer

The printer frame and extruder were successfully coupled resulting in a machine capable of 3D printing WSSCs. The main components of the 3D printer are shown in Figure 6-1.

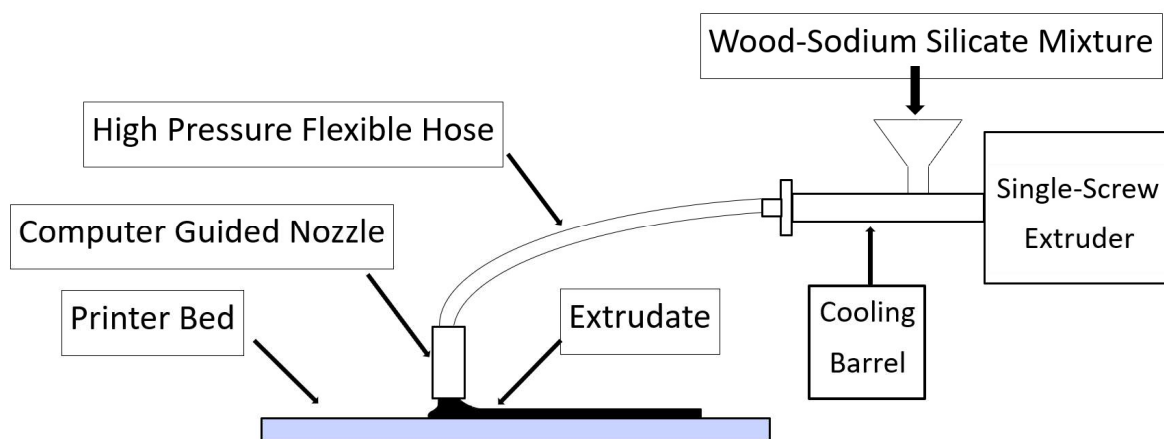


Figure 6-1: Schematic representation of 3D printer for WSSC.



Figure 6-2: Photograph of 3D printer for WSSC.

## 6.2 Extrudate Characteristics

The consistency of the WSSC is not comparable to that of concrete or PLA used in AM. The WSSC has a high viscosity and is self-supporting. The Table 6-1 shows the data taken for five pieces of printed composite. The average density of the printed composite was calculated to be 1225 kg/m<sup>3</sup>. This is comparable to the compressed composite density of 1250 kg/m<sup>3</sup> from the plunge extruder [6].

*Table 6-1: Density of extruded WSSC.*

Sample Number	L (mm)	W (mm)	H (mm)	Weight (g)	Density kg/m <sup>3</sup>
1	39.37	45.19	6.58	14.04	1199.8
2	41.07	44.93	6.65	15.12	1231.3
3	41.20	44.96	6.60	14.82	1212.0
4	40.39	45.01	6.63	14.96	1241.6
5	41.66	44.96	6.68	15.56	1243.8

Due to the spinning of the screw, the fibers of the extruded rods are oriented in a spiral pattern around the central axis. The fiber orientation of the extruded rods is shown in Figure 6-3. After deformation of the WSSC in the nozzle it is observed that the fiber orientation remains intact and deforms with the shape. The orientation of the fibers in the rectangular extrudate are shown in Figure 6-4.



*Figure 6-3: Fiber configuration of round extrudate.*



*Figure 6-4: Fiber configuration of rectangular extrudate.*

After storage of 24 hours at room temperature and in the freezer, both batches of WSSC failed to retain the same consistency as the freshly mixed WSSC and failed to extrude.



*Figure 6-5: (A) Fresh extrudate. (B) Extrudate held at room temperature. (C) Extrudate stored in freezer.*

The addition of water of any amount was found to not extrude and become backed up inside the extruder barrel. The addition of 1% water of the total weight is shown in Figure 6-6 filling the barrel completely to the feeder.





*Figure 6-6: Water added to mixture unable to extrude.*

The addition of water to the WSSC also produced a sap-like substance leaving the die nozzle. Figure 6-7 shows the sap-like substance leaking from between the die and extruder barrel as well as out the exit. The WSSC with added water is unable to exit the die causing the liquid to be squeezed out and separate from the wood instead of being extruded.



*Figure 6-7: Sodium silicate and water mix leaking from die.*

After curing, it was observed that the tap water WSSC had bowed significantly due to uneven drying. The hand mixed WSSC did not have any deformations during curing. The binder jetting also displayed no observable deformation during curing. Figure 6-8 shows the three mixtures in the oven after 48 hours at 105°C.



Figure 6-8: (Left) Liquid mixture (Center) Hand Mixed (Right) Binder Jetting

Upon removing the parchment paper from the back of the water WSSC, the sample crumbled into multiple pieces. Figure 6-9 is a picture of the mixture before and after breaking.



Figure 6-9: (Left) Cured mixture with water added. (Right) Broken wood composite.

Once cured the binder jetting mixture was removed from the oven and any excess wood-flour was removed. The binder jetting mixture's remaining material was left in the same pattern as the deposited binder before curing. The wood flour did not absorb the sodium silicate leaving a brittle piece with very few wood fibers shown in Figure 6-10.



*Figure 6-10: Ink jetting of sodium silicate onto wood flour.*

The green food coloring showed minimal mixing happening inside the extruder barrel. The mixing of the color was limited to the outside surface of the extrudate. Figure 6-11 pictures the extrudate with minimal internal mixing of the green food coloring.



*Figure 6-11: Extrudate with added green food coloring.*

The interaction of the WSSC as it leaves the nozzle and is deposited onto the printer bed is shown in Figure 6-12. The WSSC undergoes a deformation after being extruded. This sample had a 45:55 wood to sodium silicate weight ratio and was found to be the best ratio for layer adhesion.

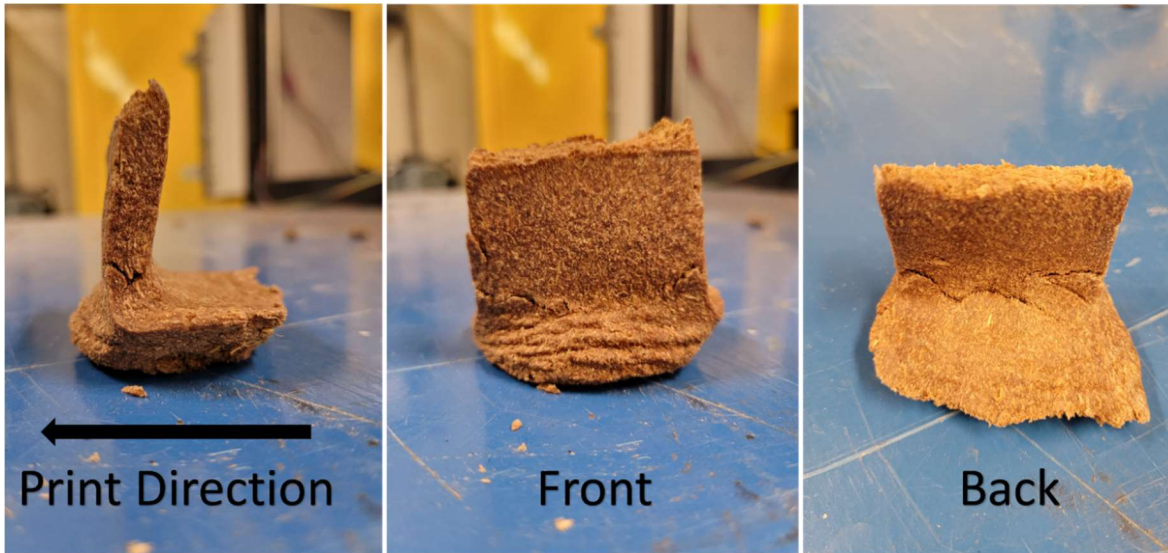


Figure 6-12: (Left) Side view of extrudate interaction with bed. (Center) Front view. (Right) Back view.

### 6.3 Interlayer Adhesion

After curing at room temperature for 11 days, no chemical or mechanical bond between the extruded segments was present. The different segments retained their shape, but were easily removed by hand and separated at the boundary layers. Figure 6-13 shows the compressed sample after curing and being broken apart.



Figure 6-13: (Left) Segment separates at boundary layer. (Right) All four sections of extrudate separated.

As the composite cured, it was observed that all of the parameters evaluated for interlayer adhesion of the WSSC begin to separate. The samples cure from the outside edges in, causing the samples to bow away from one another. Figure 6-14 shows a picture of the layers separating from one another after curing.



Figure 6-14: Failed interlayer connections

Higher pressure applied to the layers before curing resulted in lower separation of the layers. Figure 6-15 shows a picture of the four layers pressed with 0.15 Mpa (21.4 psi) of pressure and cured at 60°C for half the desired cure time of 24 hours.



*Figure 6-15: Layers separate during curing.*

During curing, all of the layers of the 90-degree layer orientation specimen separated and was only touching in some locations.

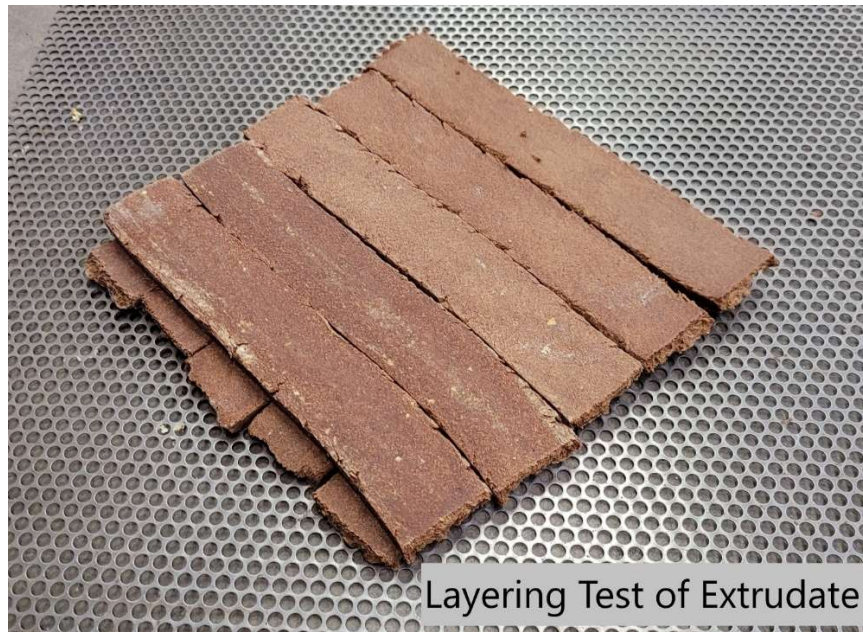


Figure 6-16: Cross layering

A studded wall print 381 mm by 458 mm with one stud was completed. Figure 6-17 shows a photo of the stud wall printed with a nozzle and print bed height,  $H_B$ , of 22 mm and nozzle head velocity,  $V_N$ , of 58 mm/min.



Figure 6-17: 3D printed material in both X and Y directions.

Side-by-side layering was achieved using a 45:55 wood to sodium silicate weight ratio and a nozzle velocity,  $V_N$ , of 58 mm/min, a layer height,  $H_L$ , of 26 mm and center distance,  $D_L$ , of 42 mm.



Figure 6-18: Side-by-side layering of WSSC with interlayer adhesion. (Left) Top. (Right) Bottom.

The WSSC side-by-side layers were cured at 60°C for 48 hours. This combination of printing and curing parameters adhered the interlayers for the WSSC and breaking occurred away from the layer boundary.



Figure 6-19: Failure occurred in the base material not at layer boundary.

A single layer panel, 610 mm long by 458 mm wide, was printed. It was found that using a 45:55 wood to sodium silicate weight ratio gave the best interlayer adhesion. Figure 6-20 shows a picture of the panel on the print bed before curing.





Figure 6-20: 3D printed panel.

### 6.4 Water Soak Test

After soaking the WSSC samples for 24 hours it was found that the samples that were cured at room temperature and 60°C fully dissolved in the water. Figure 6-21 shows the dissolved WSSC. The WSSC cured at 106°C retained its shape and did not dissolve. Figure 6-22 shows the weight and thickness percentage change for the water soaked WSSC.



Figure 6-21: Dissolved WSSC cured at room temperature.

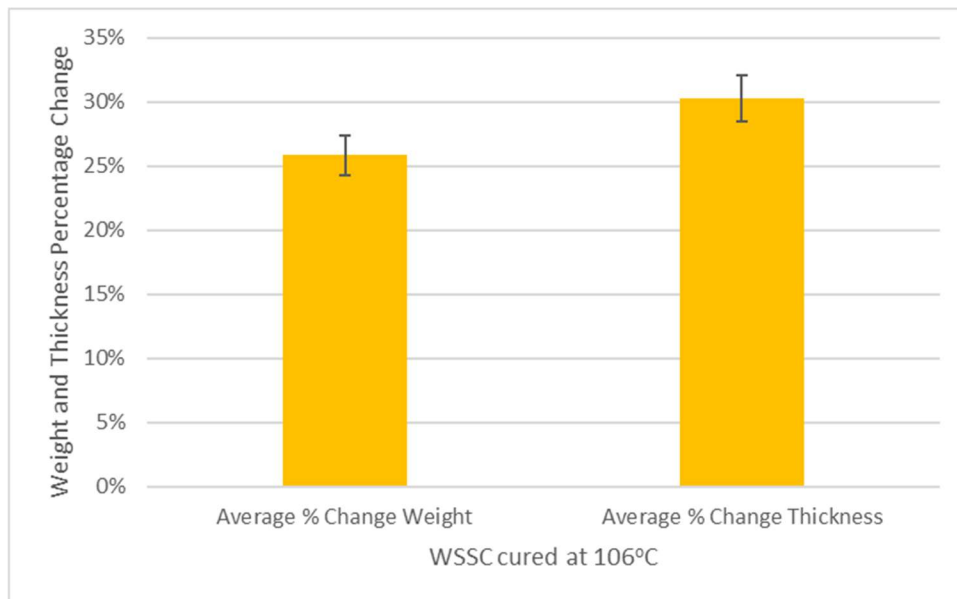


Figure 6-22: Average percentage change of weight and thickness of panel samples before and after soaking.

## Chapter 7: Summary and Conclusions

### 7.1 Summary

The use of AM is growing rapidly in the construction industry. Using AM in construction applications can reduce waste and allows for the optimization of geometry not possible with other building techniques. Concrete is currently being used as the primary feedstock for this application. Although wood-based composites are well-established in the construction industry, producing them using AM techniques for construction applications has yet to be fully developed. Traditionally, wood-based composites have high wood content and require a both high pressure and heat to produce a product that is cost effective yet has properties suitable for building. However, high strength wood composites using AM are difficult to produce with a traditional additive manufacturing process.

A new method has been developed to use wood-based composites in AM. This method utilizes screw extrusion to provide a continuous material flow and a new AM technique called Bio-Composite Additive Manufacturing (BCAM) providing high pressure deposition and shaping of the material.

Understanding the characteristics of the wood-based composite is critical to its use in AM. Sodium silicate was the resin used in the composite. Utilizing a thermoset resin as the composite's adhesive allows the composite to extrude in a semi-fluid state while still hardening afterwards into a strong construction material.

This study discussed the design and implementation of a custom 3D printer for WSSC. The purpose of developing a 3D printer was for its use in using wood-based composites in AM. The transportation, deposition, and adhesion of the wood-based composite was analyzed during extrusion/printing, and the interlayer adhesion and material characteristics were assessed once the composite had cured. Various parameters of the composite were tested, including wood to resin ratio, layer height, nozzle speed, and curing method.

## 7.2 Conclusions

Wood-based composites for construction have not typically been produced using AM. The AM techniques available today do not have the capabilities to 3D print such high strength wood-based composites, thus a 3D printer and wood-based AM technique had to be designed and produced. To 3D print a wood-based composite, a reinforced printer frame coupled to a single screw extruder was used. The printing process performed best while using a 55:45 wood to sodium silicate weight ratio with a non-compression screw at 40 rpm. Additionally, the extruder performed best while using the cooling barrel to minimize premature curing of the thermoset resin.

It was discovered that the extruded WSSC would not adhere to itself using any additional additives. The samples that produced the best bed adhesion were those with a nozzle and print bed height,  $H_B$ , of 22 mm and nozzle head velocity,  $V_N$ , of 58 mm/min. It was also discovered that samples manufactured using the V5 nozzle with a nozzle head velocity  $V_N$ , of 58 mm/min, a layer height,  $H_L$ , of 22 mm, and distance between the center of each printed layer  $D_L$ , of 40 mm produced the best interlayer adhesion.

It was found that curing temperatures greatly affected the composite's ability to resist water. Samples cured above 106°C were found to have the best water resistance. Additionally, curing temperature affected the level of warping and shrinkage seen of the printed samples. Minimal shrinkage and warping were observed in specimens cured at 60°C.

## Chapter 8: Future Work

The purpose of this research was to give proof of concept of the methodology of a process to be able to use 3D printing in construction applications using waste wood elements and sodium-silicate. The final outcome of the research is to develop a reliable process for 3D printing house walls, floors, and roofs on a horizontal printing bed. This process can then be used to manufacture modular residential homes for low cost or provide other opportunities.

If the 3D printer were to be built again the use of angle iron would be replaced with 80/20 T-slot framing to allow for small adjustments to ensure the printer is always squared. The chemical braded hose would no longer be used and a new gear box with the ability to be mounted vertically on top of the X-axis of the printer would be implemented. The print bed would also change to be stationary and resting on the ground to minimize flexing caused from the high pressure between the WCCS and bed.

Future work using wood in AM for construction purposes should entail further development of the extruded material properties and possible building applications. Using the 3D printer, large scale composite prints should be made and tested. A twin-screw extruder could be used to continuously mix the wood flour and resin mixture in the printing process. The use of a twin screw would also allow for continuous feeding of the material into the barrel and move away from a batch mixing system. During 3D printing, the use of a circular cross section nozzle exit could be used to allow layering of the material in all directions without the need to rotate the print head. The study of the effect of the layer height and nozzle speed on interlayer adhesion should be continued, including the side-by-side layering of the extruded material. The effects of curing conditions on the samples post curing shape should be explored. The fire and water resistance of the composite should also be further explored.

## References

- [1] S. M. E. Sepasgozar, A. Shi, L. Yang, S. Shirowzhan, and D. J. Edwards, "Additive Manufacturing Applications for Industry 4.0: A Systematic Critical Review," *Buildings*, vol. 10, no. 12, Art. no. 12, Dec. 2020, doi: 10.3390/buildings10120231.
- [2] "The Transformative Power of Building Information Modeling," *BCG Global*, Aug. 19, 2020. <https://www.bcg.com/publications/2016/engineered-products-infrastructure-digital-transformative-power-building-information-modeling> (accessed Jun. 15, 2022).
- [3] C. Thie, "Wood and Resin Composite Extrusion for Additive Manufacturing."
- [4] B. Buschmann, K. Henke, D. Talke, B. Saile, C. Asshoff, and F. Bunzel, "Additive Manufacturing of Wood Composite Panels for Individual Layer Fabrication (ILF)," *Polymers*, vol. 13, no. 19, Art. no. 19, Jan. 2021, doi: 10.3390/polym13193423.
- [5] C. Ahn, W. Pan, S. Lee, and F. Peña-Mora, "Enhanced estimation of air emissions from construction operations based on discrete-event simulation," p. 8.
- [6] Aina, O. M. "Wood waste utilization for energy generation." Proceedings of the international conference on renewable energy for developing countries. Forestry Bangkok, 2006.
- [7] D. Lee, H. Kim, J. Sim, D. Lee, H. Cho, and D. Hong, "Trends in 3D Printing Technology for Construction Automation Using Text Mining," *Int. J. Precis. Eng. Manuf.*, vol. 20, no. 5, pp. 871–882, May 2019, doi: 10.1007/s12541-019-00117-w.
- [8] "Additive manufacturing: Challenges, trends, and applications - Osama Abdulhameed, Abdulrahman Al-Ahmari, Wadea Ameen, Syed Hammad Mian, 2019." <https://journals.sagepub.com/doi/full/10.1177/1687814018822880#bibr7-1687814018822880> (accessed Jun. 15, 2022).
- [9] T. T. Wohlers and Wohlers Associates, *Wohlers report 2012: additive manufacturing and 3D printing state of the industry : annual worldwide progress report*. Fort Collins, Col.: Wohlers Associates, 2012.
- [10] "Additive Manufacturing of 3D Structures Composed of Wood Materials - Kam - 2019 - Advanced Materials Technologies - Wiley Online Library." [https://onlinelibrary.wiley.com/doi/full/10.1002/admt.201900158?casa\\_token=hGy79ZwbRdcAAAA%3AKpS3vT6mqYAFwjST4HD4A-MC-h5gK32SGr5yqraaj9vtpX6uAPXDBPxBPUwKeC1ET3HsuSmyYFTjKZ28](https://onlinelibrary.wiley.com/doi/full/10.1002/admt.201900158?casa_token=hGy79ZwbRdcAAAA%3AKpS3vT6mqYAFwjST4HD4A-MC-h5gK32SGr5yqraaj9vtpX6uAPXDBPxBPUwKeC1ET3HsuSmyYFTjKZ28) (accessed Jun. 15, 2022).
- [11] S. A. Adekanye, R. M. Mahamood, E. T. Akinlabi, and M. G. Owolabi, "Additive manufacturing: the future of manufacturing," *Mater. Tehnol.*, vol. 51, no. 5, pp. 709–715, Oct. 2017, doi: 10.17222/mit.2016.261.
- [12] R. Shmulsky and P. D. Jones, *Forest products and wood science: an introduction*, 6th ed. Chichester, West Sussex, U.K. ; Ames, Iowa: Wiley-Blackwell, 2011.
- [13] "Natural Fibers for Sustainable Bio-Composites | IntechOpen." <https://www.intechopen.com/chapters/57267> (accessed Jun. 15, 2022).
- [14] S. Lim *et al.*, "Fabricating construction components using layer manufacturing technology," *Proc Int Conf Glob Innov Constr*, pp. 512–520, Jan. 2009.
- [15] "Robotic Construction by Contour Crafting: The Case of Lunar Construction - Neil Leach, Anders Carlson, Behrokh Khoshnevis, Madhu Thangavelu, 2012." <https://journals.sagepub.com/doi/pdf/10.1260/1478-0771.10.3.423> (accessed Jun. 15, 2022).
- [16] I. Hager, A. Golonka, and R. Putanowicz, "3D Printing of Buildings and Building Components as the Future of Sustainable Construction? - ScienceDirect." <https://www.sciencedirect.com/science/article/pii/S1877705816317453> (accessed Jun. 15, 2022).

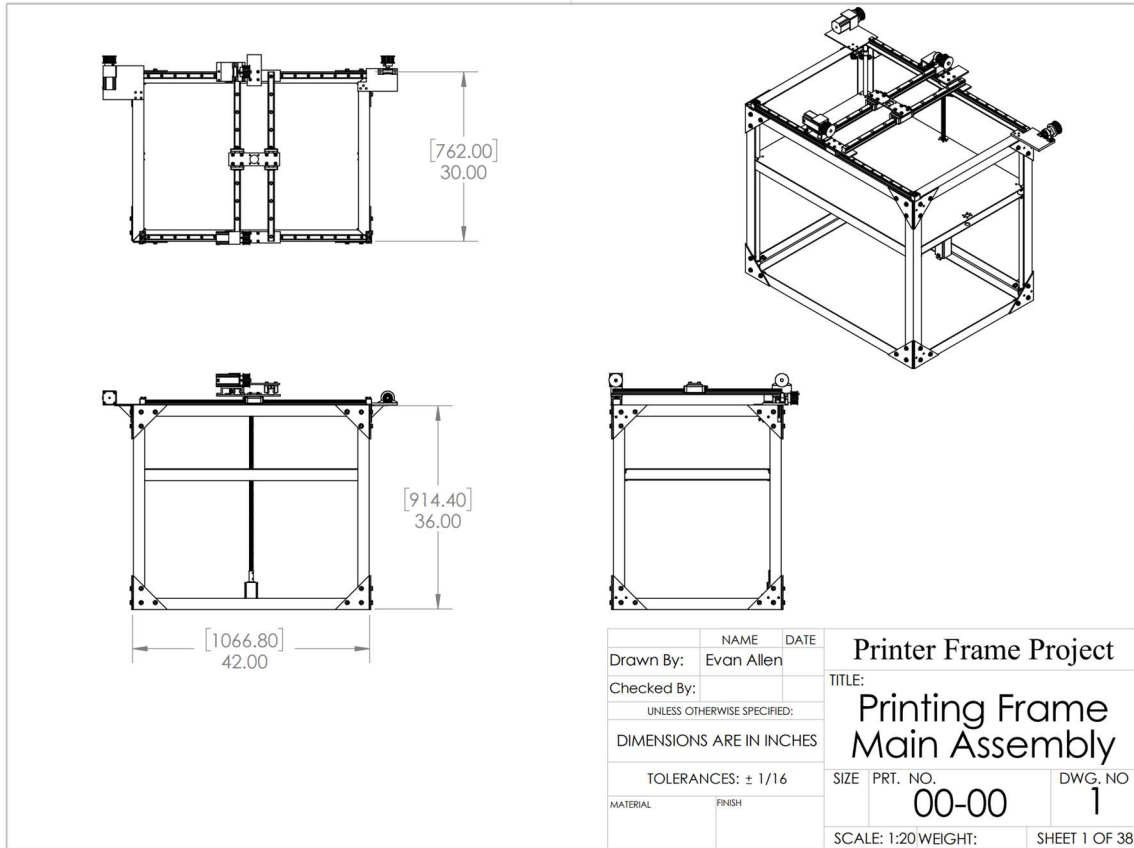
- [17] “Rudenko 3D Printer,” *Andrey Rudenko*. <http://www.totalkustom.com/gallery.html> (accessed Jun. 15, 2022).
- [18] “D-Shape Enterprises L.L.C.,” *D-Shape Enterprises L.L.C.* <https://dshape.wordpress.com/> (accessed May 31, 2022).
- [19] “Products,” *BRANCH TECHNOLOGY*. <https://branchtechnology.com/products/> (accessed Jun. 15, 2022).
- [20] T. Sakai, “Screw extrusion technology — past, present and future,” *Polimery*, vol. 58, no. 11–12, Art. no. 11–12, Dec. 2013.
- [21] “Manufacturing Processes for Engineering Materials | Manufacturing | Industrial, Biomedical & Materials | Science & Engineering | Store | Learner US Site.” <https://www.pearson.com/store/p/manufacturing-processes-for-engineering-materials/P100001424648/9780134290553> (accessed Jun. 15, 2022).
- [22] B. H. Batchelor, *Physics of plastics*. Hanser, 1992.
- [23] D. R. Heldman, *Encyclopedia of Agricultural, Food, and Biological Engineering (Print)*. CRC Press, 2003.
- [24] “G Code CNC Basic Programming: Mastering CNC Machines,” *Fictiv*. <https://www.fictiv.com/articles/g-code-knowledge-is-key-to-mastering-any-cnc-machine> (accessed May 24, 2022).
- [25] K. R. G. Punhagui and V. M. John, “Carbon dioxide emissions, embodied energy, material use efficiency of lumber manufactured from planted forest in Brazil,” *J. Build. Eng.*, vol. 52, p. 104349, Jul. 2022, doi: 10.1016/j.job.2022.104349.
- [26] J. Gardan, D. C. Nguyen, L. Roucoules, and G. Montay, “Characterization of Wood Filament in Additive Deposition to Study the Mechanical Behavior of Reconstituted Wood Products,” *J. Eng. Fibers Fabr.*, vol. 11, no. 4, p. 155892501601100400, Dec. 2016, doi: 10.1177/155892501601100408.
- [27] J. A. Travieso-Rodriguez, R. Jerez-Mesa, J. Llumà, G. Gomez-Gras, and O. Casadesus, “Comparative study of the flexural properties of ABS, PLA and a PLA–wood composite manufactured through fused filament fabrication,” *Rapid Prototyp. J.*, vol. 27, no. 1, pp. 81–92, 2021, doi: 10.1108/RPJ-01-2020-0022.
- [28] J. Durlan, B. Adrover, M. D. Zandi, J. Lluma, R. Jerez, and J. A. Travieso, “Finite element modelling and evaluation of mechanical properties of wood-PLA parts manufactured through Fused Filament Fabrication,” *IOP Conf. Ser. Mater. Sci. Eng.*, vol. 1193, no. 1, p. 012094, Oct. 2021, doi: 10.1088/1757-899X/1193/1/012094.

## Appendix A – G-code Commands

G-Code	Description	Example
G0	Move to the given coordinates. To the contrary of G1, if there is a tool it will most of the time be off during this kind of move. This is a “go to” move rather than a “do while going to” move. The F parameter defines speed and is remembered by subsequent commands ( specified in millimetres/minute ) (command is modal)	G0 X10 Y5 F100
G1	Move to the given coordinates, see above for difference with G0. Takes the same F parameter as G0. (command is modal)	G1 X20 Y2.3 F200
G2	Clockwise circular motion : go to point with coordinates XYZ while rotating around point with relative coordinates IJ (command is not modal)	G2 X10 J5
G3	Counter-clockwise motion : see above (command is not modal)	G3 Y5 X10 I2
G4	Dwell S<seconds> or P<milliseconds>, In grbl mode P is float seconds to comply with gcode standards	G4 P1000
G10	Do firmware extruder retract	G10
G11	Do firmware extruder un-retract	G11
G10 L1	Set extruder tool offset for specified extruder where Pn is the extruder number + 1 (T0 is P1, T1 is P2), This stays set until reset. Permanent change must be added to config, Only active when multiple extruders have been defined	G10 L1 P2 X10
G10 L2, G10 L20	Set workspace coordinates <a href="http://linuxcnc.org/docs/html/gcode/coordinates.html">http://linuxcnc.org/docs/html/gcode/coordinates.html</a> and <a href="http://linuxcnc.org/docs/html/gcode/g-code.html#gcode:g10-l2">http://linuxcnc.org/docs/html/gcode/g-code.html#gcode:g10-l2</a>	G10 L2 P1 X0
G17	Select XYZ plane (command is modal)	G17
G18	Select XZY plane (command is modal)	G18
G19	Select YZX plane (command is modal)	G19
G20	Inch mode : passed coordinates will be considered as inches, so internally translated to millimeters (command is modal)	G20
G21	Millimeter mode ( default ) : passed coordinates will be considered as millimeters (command is modal)	G21
G28	Home The given axis, or if no axis specified home all axis at the same time (edge) NOTE in CNC/grbl mode this is move to park position, use \$H to home	G28
G28.1	Set Predefined Position - This position will be returned to by G28.2	G28.1
G28.2	Move to Predefined Position - This perform a rapid move to the Predefined position set by G28.1 (in grbl mode this will do a home)	G28.2
G28.3	Manual Homing - This allows you to set a home position manually without moving to limit switches	G28.3
G28.4	Manual Homing based on actuator position- This allows you to set a home position manually based on actuator position (used for rotary delta)	G28.4
G28.5	Clears the homed flag for the specified axis, or all if not specified	G28.5 G28.5 Z0
G28.6	Shows the homing status of each axis	G28.6
G29	Probes the bed and outputs the bed heights depending on levelling strategy selected, see ZProbe	G29
G30	Simple Z probe at current XY, reports distance moved down until probe triggers. optional F parameter defines the speed of probing, zprobe.slow_feedrate is used when not supplied	G30 G30 F100
G31	Depends on levelling strategy selected, see ZProbe	G31
G32	Depends on levelling strategy selected, see ZProbe. For calibration on delta, uses Z probe to calibrate delta endstops and arm radius, use R parameter to select only arm radius calibration and E to select only endstop calibration. I to set target precision, J to set probe_radius, K to keep current endstop trim settings. In Zgrid module, it starts the grid probing	G32 G32 R G32 E G32 EK G32 I0.02
G38.2 G38.3 G38.4 G38.5	Standard probe commands implemented as documented here	G38.2 Z-10
G43.2	Baby steps	G43.2 Z0.05
G53	Must be on a line by itself OR the first G code on a line, the directly following G0/G1 will be executed in MCS coordinates	G53 G0 X0 Y0
G54-G59.3	use workspace coordinates <a href="http://linuxcnc.org/docs/html/gcode/coordinates.html">http://linuxcnc.org/docs/html/gcode/coordinates.html</a> and <a href="http://linuxcnc.org/docs/html/gcode/g-code.html#gcode:g54-g59.3">http://linuxcnc.org/docs/html/gcode/g-code.html#gcode:g54-g59.3</a>	G54
G90	Absolute mode ( default ) (command is modal)	G90
G91	Relative mode (command is modal)	G91
G92	Set global workspace coordinate system to specified coordinates <a href="http://linuxcnc.org/docs/html/gcode/g-code.html#gcode:g92">http://linuxcnc.org/docs/html/gcode/g-code.html#gcode:g92</a>	G92 X0 Y0 Z0
G92.1	Clear the G92 and G30 Znnn offsets	G92.1
G92.4	manually set homing (MCS) for XYZ	G92.4 X0 Y0 Z0



### Appendix B – Printer Frame



ITEM NO.	Sub-Assembly NO.	DESCRIPTION	QTY.
1	01-00	Frame Sub-Assembly	1
2	02-00	Z-Axis Platform Assembly	1
3	03-00	X-Y Axis Assembly	1

NAME		DATE		<b>Printer Frame Project</b>	
Drawn By: Evan Allen					
Checked By:				TITLE:	
UNLESS OTHERWISE SPECIFIED:				<b>Printing Frame</b>	
DIMENSIONS ARE IN INCHES				<b>Main Assembly</b>	
TOLERANCES: ± 1/16		SIZE	PRT. NO.	DWG. NO.	
MATERIAL		00-00		2	
FINISH				SCALE: 1:20 WEIGHT: SHEET 2 OF 38	

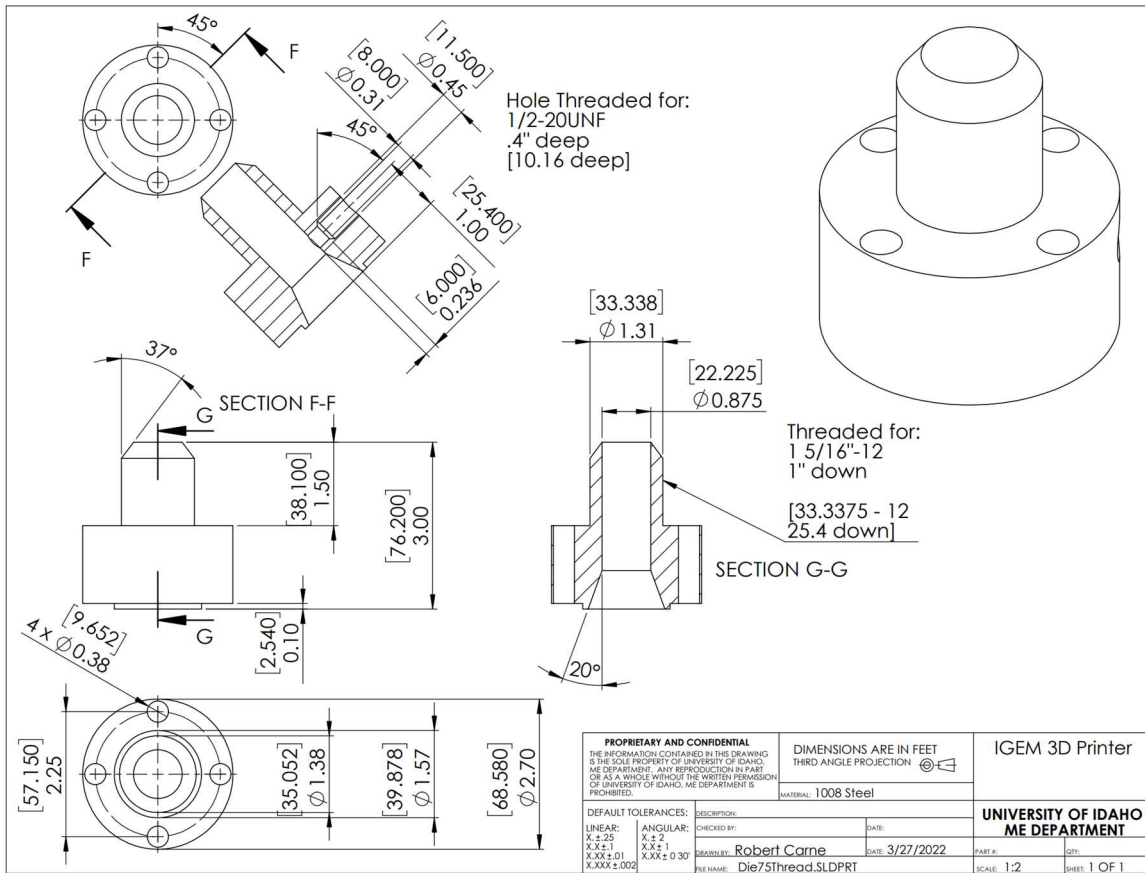
## Appendix C – Braided Hose Specifications

Component	Hose
For Use With	Mineral Oil, Toluene
Temperature Range	-40° to 350° F
Connection Type	Hose
Hose Connection Type	Without Fittings
ID	7/8"
OD	1"
Bend Radius	9"
Maximum Pressure	1,000 psi @ 72° F
Maximum Vacuum	14" of Hg @ 72° F
For Use Outdoors	Yes
Material	PTFE
Braid Material	304 Stainless Steel
Interior Texture	Smooth
External Reinforcement	Braided
Maximum Continuous Length	50 ft.
RoHS	RoHS 3 (2015/863/EU) Compliant
REACH	Not Compliant
DFARS	Specialty Metals COTS-Exempt
Country of Origin	United States
USMCA Qualifying	No
Schedule B	391731
ECCN	EAR99

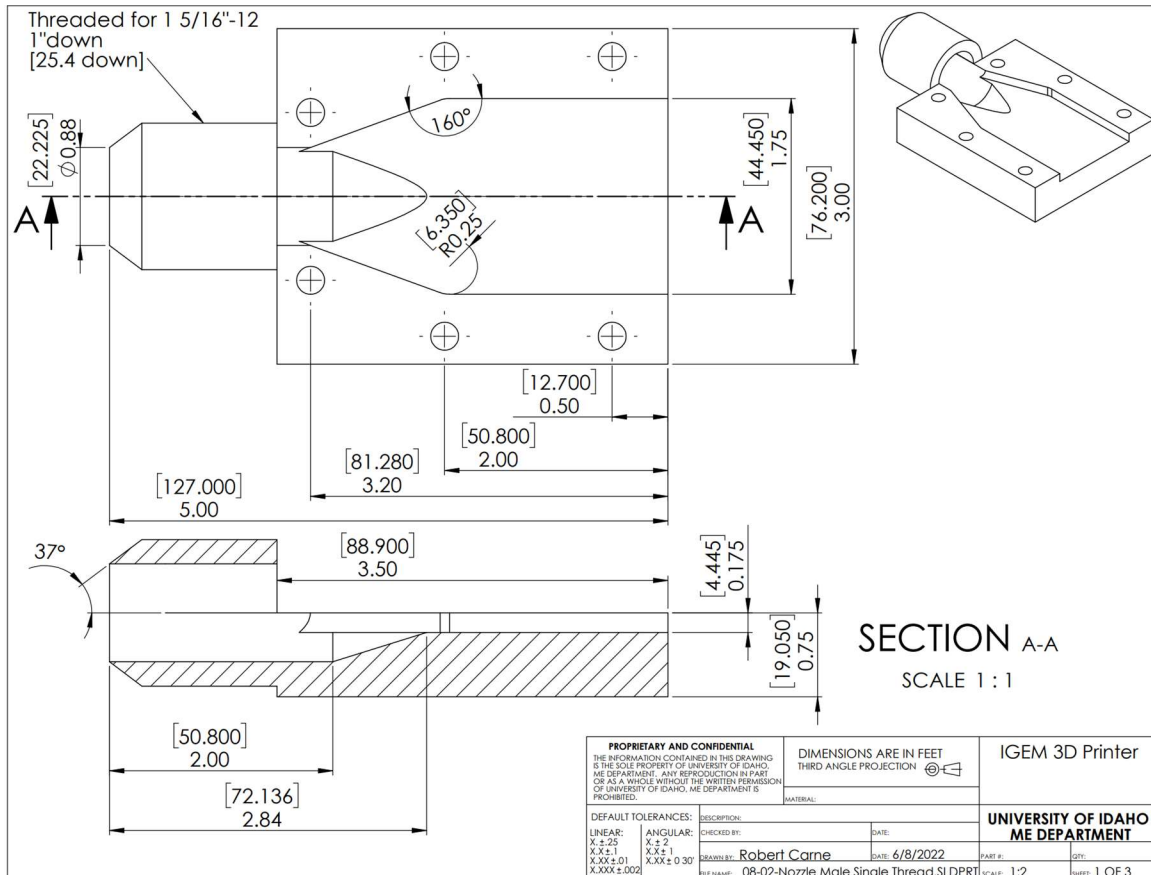
## Appendix D – JIC Fitting Specifications

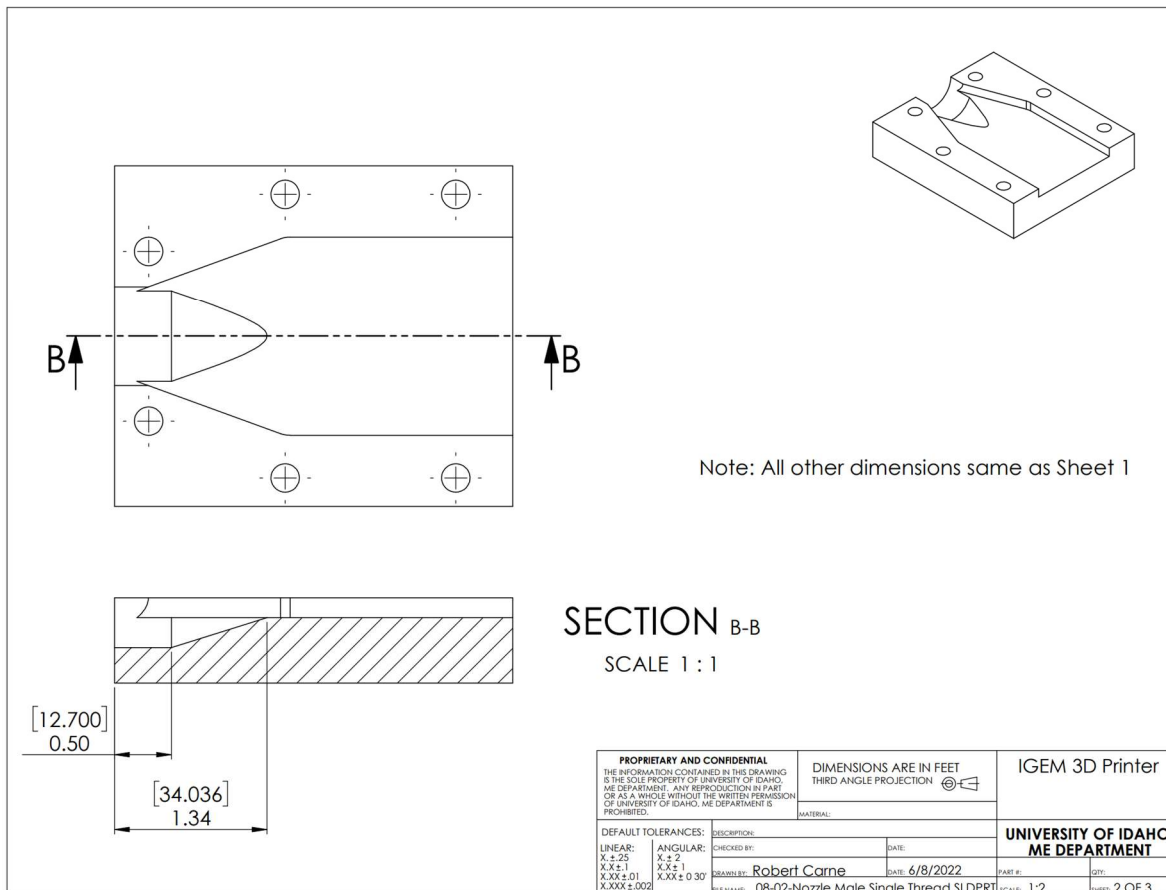
Component	Fitting
For Use With	Mineral Oil, Toluene
Temperature Range	-40° to 350° F
Connection Type	Tube
Connection	37° Flared UNF Female (Swivels Until Tightened)
For Hose ID	7/8"
Thread Size	1 5/16"-12
click to learn more about	click to learn more about 1 5/16"-12
Maximum Pressure	1,000 psi @ 72° F
Material	Brass
Nut Material	Zinc-Plated Steel
For Use Outdoors	Yes
Specifications Met	SAE J514, MS27070, MS27075
RoHS	RoHS 3 (2015/863/EU) Compliant
REACH	REACH (EC 1907/2006) (07/08/2021, 219 SVHC) Compliant
DFARS	Specialty Metals COTS-Exempt
Country of Origin	United States
USMCA Qualifying	No
Schedule B	741980.55
ECCN	EAR99

### Appendix E – Threaded Die



### Appendix F – V5 Nozzle

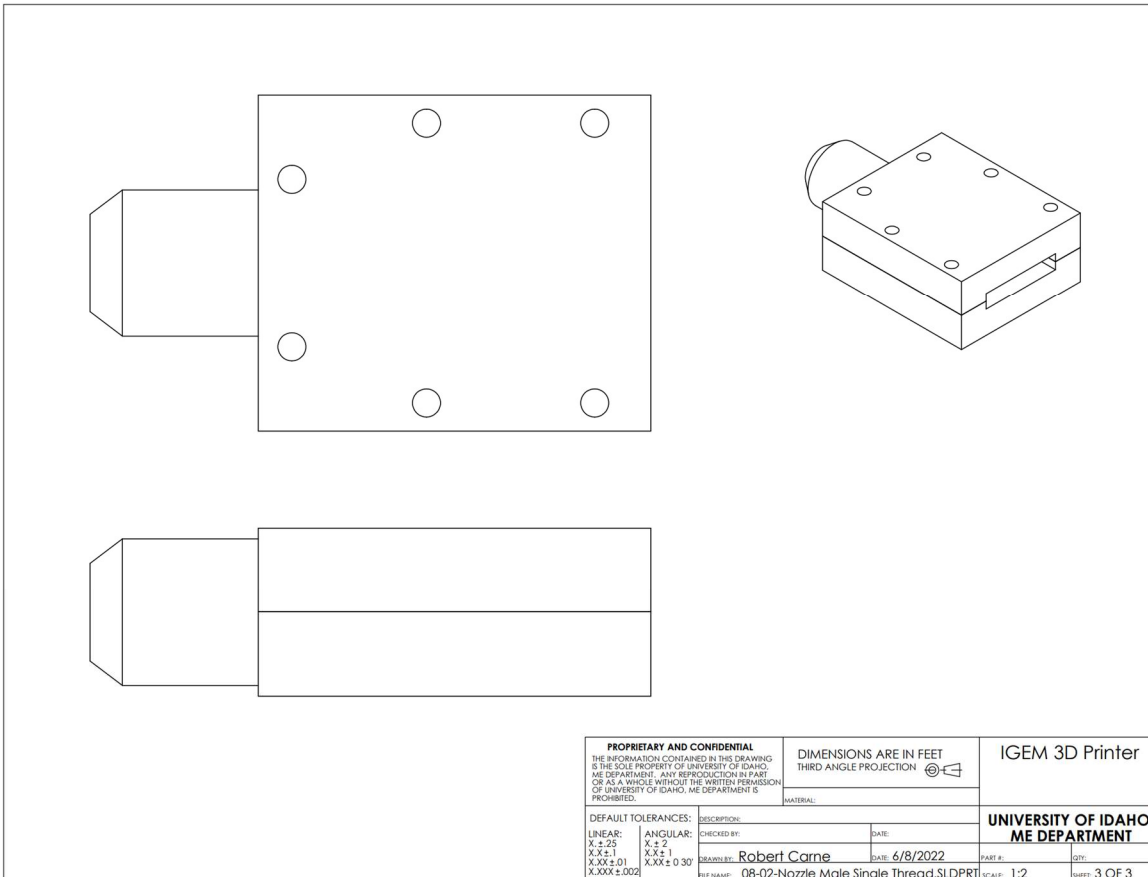




Note: All other dimensions same as Sheet 1

**SECTION B-B**  
SCALE 1 : 1

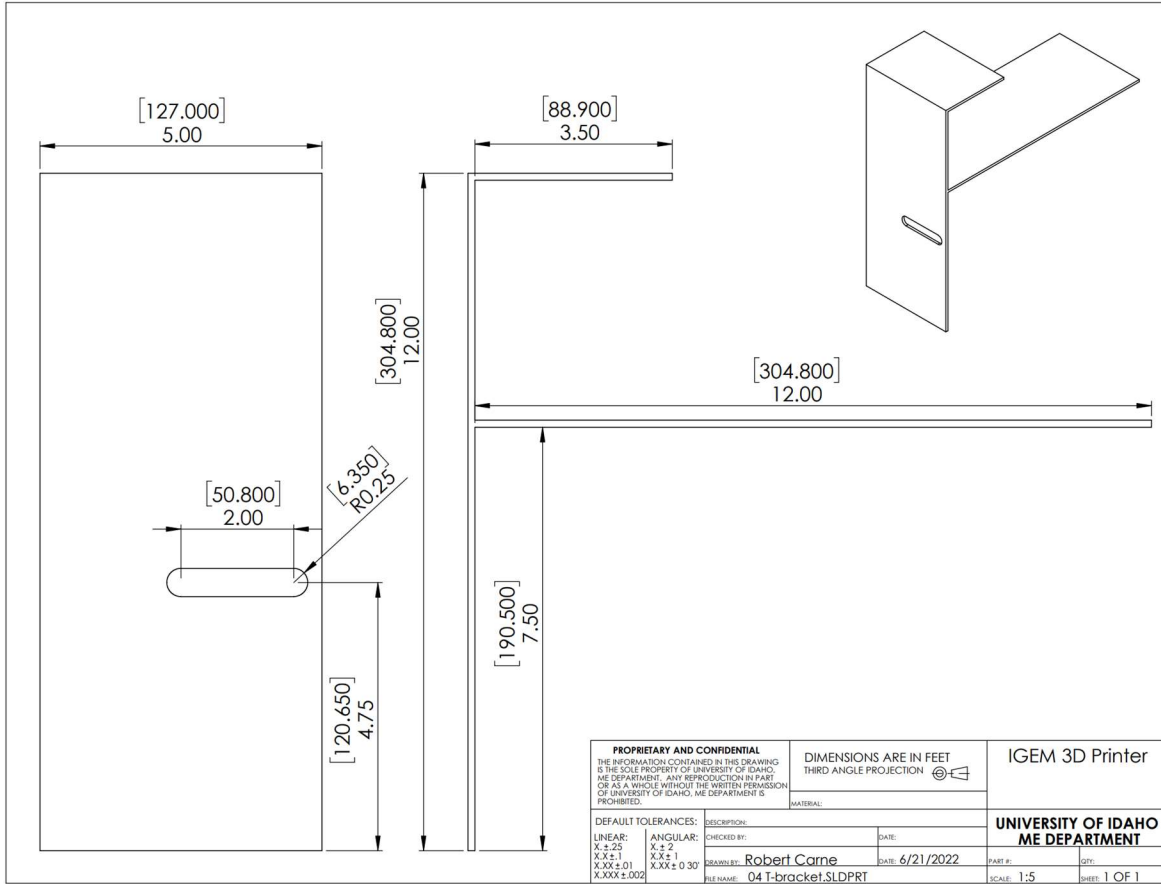
<b>PROPRIETARY AND CONFIDENTIAL</b> THE INFORMATION CONTAINED IN THIS DRAWING IS THE SOLE PROPERTY OF UNIVERSITY OF IDAHO, ME DEPARTMENT. ANY REPRODUCTION IN PART OR AS A WHOLE WITHOUT THE WRITTEN PERMISSION OF UNIVERSITY OF IDAHO, ME DEPARTMENT IS PROHIBITED.		DIMENSIONS ARE IN FEET THIRD ANGLE PROJECTION		IGEM 3D Printer	
DEFAULT TOLERANCES:		MATERIAL:		UNIVERSITY OF IDAHO ME DEPARTMENT	
LINEAR: X ± .25 X.X ± .1 X.XX ± .01 X.XXX ± .002	ANGULAR: X ± 2 X.X ± 1 X.XX ± 0.30	DESCRIPTION:	CHECKED BY:	DATE:	PART #:
		DRAWN BY: Robert Carne		DATE: 6/8/2022	QTY:
		FILE NAME: 08-02-Nozzle Male Single Thread.SLDPR	SCALE: 1:2	SHEET: 2 OF 3	



<b>PROPRIETARY AND CONFIDENTIAL</b> THE INFORMATION CONTAINED IN THIS DRAWING IS THE SOLE PROPERTY OF UNIVERSITY OF IDAHO ME DEPARTMENT. ANY REPRODUCTION IN PART OR AS A WHOLE WITHOUT THE WRITTEN PERMISSION OF UNIVERSITY OF IDAHO, ME DEPARTMENT IS PROHIBITED.		DIMENSIONS ARE IN FEET THIRD ANGLE PROJECTION		IGEM 3D Printer	
DEFAULT TOLERANCES:		DESCRIPTION:		MATERIAL:	
LINEAR:	ANGULAR:	CHECKED BY:	DATE:	<b>UNIVERSITY OF IDAHO ME DEPARTMENT</b>	
X ± .25	X ± 2				
X.X ± .1	XX ± 1	DRAWN BY: Robert Carne	DATE: 6/8/2022	PART #:	QTY:
X.XX ± .01	X.XX ± 0.30	FILE NAME: 08-02-Nozzle Male Single Thread.SLDPRT	SCALE: 1:2		SHEET: 3 OF 3
X.XXX ± .002					



### Appendix G – Rotating Head Bracket



## Appendix H – Config. File for SmoothieBoard

```

# Basic motion configuration
default_feed_rate    4000 # Default speed (mm/minute) for G1/G2/G3 moves
default_seek_rate    3000 # Default speed (mm/minute) for G0 moves
mm_per_arc_segment   0.0 # Fixed length for line segments that divide arcs, 0 to disable
#mm_per_line_segment .1 # # Cut lines into segments this size
mm_max_arc_error     0.01 # The maximum error for line segments that divide arcs 0 to disable
                        # Note it is invalid for both the above be 0
                        # If both are used, will use largest segment length based on
                        radius
                        # Arm solution configuration : Cartesian robot. Translates
                        mm   positions into stepper positions

alpha_steps_per_mm   640 # Steps per mm for alpha ( X ) stepper
beta_steps_per_mm    640 # Steps per mm for beta ( Y ) stepper
gamma_steps_per_mm   400 # Steps per mm for gamma ( Z ) stepper

# Planner module configuration : Look-ahead and acceleration configuration

#planner_queue_size          10
acceleration      500 # Acceleration in mm/second/second.
gamma_acceleration 300 # Acceleration for Z only moves in mm/s^2, 0 uses acceleration
                        which is the default. DO NOT SET ON A DELTA

junction_deviation  0.1 # See http://smoothieware.org/motion-control#junction-deviation
#z_junction_deviation 0.0 # For Z only moves, -1 uses junction_deviation, zero disables
junction_deviation on z moves DO NOT SET ON A DELTA

# Cartesian axis speed limits
x_axis_max_speed    5000 # Maximum speed in mm/min
y_axis_max_speed    5000 # Maximum speed in mm/min
z_axis_max_speed    3000 # Maximum speed in mm/min

```

## # Stepper module configuration

# Pins are defined as ports, and pin numbers, appending "!" to the number will invert a pin

#EN2 to EN4 # Hard wire

#ST2 to ST4 # Hard wire

#DIR2 to DIR4 # Hard wire

#EN3 to EN5 # Hard wire

#ST3to ST5 # Hard wire

#DIR3 to DIR5 # Hard wire

alpha\_step\_pin 2.0 # Pin for alpha stepper step signal

alpha\_dir\_pin 0.5 # Pin for alpha stepper direction, add '!' to reverse direction

alpha\_en\_pin 0.4 # Pin for alpha enable pin

alpha\_current 1.8 # X stepper motor current

alpha\_max\_rate 5000 # Maximum rate in mm/min

beta\_step\_pin 2.1 # Pin for beta stepper step signal

beta\_dir\_pin 0.11 # Pin for beta stepper direction, add '!' to reverse direction

beta\_en\_pin 0.10 # Pin for beta enable

beta\_current 1.8 # Y stepper motor current

beta\_max\_rate 5000 # Maximum rate in mm/min

gamma\_step\_pin 2.2 # Pin for gamma stepper step signal

gamma\_dir\_pin 0.20 # Pin for gamma stepper direction, add '!' to reverse direction

gamma\_en\_pin 0.19 # Pin for gamma enable

gamma\_current 1.9 # Z stepper motor current

gamma\_max\_rate 3000.0 # Maximum rate in mm/min

delta\_current 1.8

delta\_max\_rate 3000.0

```
epsilon_current      1.9
epsilon_max_rate     3000.0
```

```
#Switch Module for Linear Actuator 0 degrees
```

```
switch.actuator.enable      true #
switch.actuator.input_on_command  M3 #
switch.actuator.input_off_command M5 #
switch.actuator.output_pin    1.23 # Here we are using the first big MOSFET
switch.actuator.output_type   pwm # pwm output settable with S parameter in the
input_on_comand
switch.actuator.max_pwm      255 # set max pwm for the pin default is 255
```

```
#Switch Module for Linear Actuator 90 degrees
```

```
switch.actuator1.enable     true #
switch.actuator1.input_on_command  M4 #
switch.actuator1.input_off_command M6 #
switch.actuator1.output_pin    2.6 # Here we are using the first big MOSFET
switch.actuator1.output_type   pwm # pwm output settable with S parameter in the
input_on_comand
switch.actuator1.max_pwm      255 # set max pwm for the pin default is 255
```

## Appendix I – G -code for Panel

```
G0 X0 Y0 Z0 F2000
G0 Z-22
G0 X50
G4 S2
M4
G4 S5
M6
G0 X475 F58
G4 S1
G0 Z-100 F2000
G0 Z-20
G0 Z-25
G0 X50 Y40 F2000
G4 S2
G0 Z-22
G0 X475 F58
G4 S1
G0 Z-100 F2000
G0 Z-20
G0 Z-25
G0 X50 Y80 F2000
G4 S2
G0 Z-22
G0 X475 F58
G4 S1
G0 Z-100 F2000
G0 Z-20
G0 Z-25
G0 X50 Y120 F2000
G4 S2
G0 Z-22
G0 X475 F58
G4 S1
G0 Z-100 F2000
G0 Z-20
G0 Z-25
G0 X50 Y160 F2000
G4 S2
G0 Z-22
G0 X475 F58
G4 S1
G0 Z-100 F2000
G0 Z-20
```

G0 Z-25  
G0 X50 Y200 F2000  
G4 S2  
G0 Z-22  
G0 X475 F58  
G4 S1  
G0 Z-100 F2000  
G0 Z-20  
G0 Z-25  
G0 X50 Y240 F2000  
G4 S2  
G0 Z-22  
G0 X475 F58  
G4 S1  
G0 Z-100 F2000  
G0 Z-20  
G0 Z-25  
G0 X50 Y280 F2000  
G4 S2  
G0 Z-22  
G0 X475 F58  
G4 S1  
G0 Z-100 F2000  
G0 Z-20  
G0 Z-25  
G0 X50 Y320 F2000  
G4 S2  
G0 Z-22  
G0 X475 F58  
G4 S1  
G0 Z-100 F2000  
G0 Z-20  
G0 Z-25  
G0 X50 Y360 F2000  
G4 S2  
G0 Z-22  
G0 X475 F58  
G4 S1  
G0 Z-100 F2000  
G0 Z-20  
G0 Z-25  
G0 X50 Y400 F2000  
G4 S2  
G0 Z-22

G0 X475 F58  
G4 S1  
G0 Z-100 F2000  
G0 Z-20  
G0 Z-25  
G0 X50 Y440 F2000  
G4 S2  
G0 Z-22

## Appendix J – G-code for Studded Wall

```
G0 X0 Y0 Z0 F2000
G0 Z-22
G0 X10
G4 S2
G0 Y50 F2000
G4 S2
G0 Y350 F58
G4 S1
G0 Z-100 F2000
G0 Z-20
G0 Z-25
G0 X237.5 Y50 F2000
G4 S2
G0 Y350 F58
G4 S1
G0 Z-100 F2000
G0 Z-20
G0 Z-25
G0 X475 Y50 F2000
G0 Y350 F58
G4 S1
G0 Z-100 F2000
G0 Z-20
G0 Z-25
M4
G4 S5
M6
G0 X50 Y10 F2000
G0 X475 F58
G4 S1
G0 Z-100 F2000
G0 Z-20
G0 Z-25
G0 X50 Y350 F2000
G0 X475 F58
G4 S1
G0 Z-100 F2000
G0 Z-20
G0 Z-25
G0 X0 Y0 Z-500 F200
```



## Appendix K – G-code for 2X4

G0 X0 Y0 Z0 F2000  
G0 X237.5 Y50 Z-22 F2000  
G0 Y800 F28  
G0 Z-44 F200  
G0 Y50 F58  
G0 Z-66 F200  
G0 Y800 F200  
G0 Z-88 F200  
G0 Y50 F58  
G0 Z-100 F200  
G0 Y800 F58  
G0 Z-122 F200  
G0 Y50 F58